UNIVERSIDADE DE COIMBRA

Nonlinear terms and density dependence of the nuclear symmetry energy effect on neutron star structure and content

Daniel Pessoa da Silva Bizarro

Constança Providência, advisor.
Masters Degree Dissertation in Nuclear and Particle Physics
Faculty of Sciences and Technology
University of Coimbra
2013

Resumo

Neste trabalho estuda-se o efeito da energia de simetria nas propriedades de estrelas de neutrões fazendo uso de variações da parametrização NL3 à temperatura $T = 0$ K em teoria de campos relativistas com o modelo de Walecka não linear (NLWM) alterado de forma a conter termos de mistura entre os mesões ρ-σ e ρ-ω acoplados com o factor Λ_σ e Λ_ω respectivamente. De modo a fixar os acoplamentos faz-se um estudo da matéria nuclear simétrica, i.e., constituída por uma fracção igual de protões e neutrões em primeiro lugar e depois em equilíbrio β. Comparam-se os modelos com três estrelas com $1\,M_\odot$, $1.44\,M_\odot$ e $1.67\,M_\odot$. Verifica-se que o raio de uma estrela com massa fixa, maior do que uma massa solar, aumenta linearmente com declive da energia de simetria e que as variações provocadas pela mistura Λ_ω são de maior grandeza do que com a mistura Λ_σ.

Abstract

In this work we studied the effect of the symmetry energy on the properties of a neutron star using variations on the NL3 parameter set at $T = 0$ K within the framework of the relativistic non-linear Walecka model with an extra ρ-σ and ρ-ω meson interaction with the couplings Λ_σ and Λ_ω respectively. For the purpose of fixing the aforementioned couplings we first studied matter with a fixed 0.5 proton fraction. We used these values to study their implications on the star structure with a model for nuclear matter in beta equilibrium. We fixed the masses of three different stars ($1M_\odot$, $1.441M_\odot$, $1.67M_\odot$) and verified that for stars with masses above 1 $M_\odot$, the radius of the star varies linearly with the symmetry energy slope, L, and that the slope of the growth is greater with the Λ_ω coupling than with the Λ_σ coupling.

Acknowledgements

I would like to express my deep gratitude to Constança Providência, Aziz Rabhi, Pedro Costa and João Moreira.

Contents

List of Figures

List of Tables

Chapter 1

Introduction

1.1 Work description

Knowledge of the equation of state (EOS) of high density nuclear matter greatly populated by neutrons is of prime importance to get insights into the physics of compact stars [1]. Some authors [2–4] used data from the observation of compact stars to restrict the parameters of the EOS. One author [3] has used information about a set of stars to set up an empirical dense equation of state. In this work we develop the EOS in the framework of the relativistic mean field theory. These nuclear models are usually fitted to the ground-state properties of nuclei and nuclear matter saturation properties [5]. Different fits are possible, with giant resonances [6] and for twin bands in rotating super-deformed nuclei [7]. These models only work for an asymmetry smaller than 0.2 [8,9] and work better close to saturation leaving open questions for high densities, i.e. each model predicts a different neutron star with very distinct properties and there should be only one, i.e. all the models need refinement or we need to choose between one of them. In the present work we want to understand how the symmetry energy and its slope at saturation influences the mass-radius curve of a family of stars. We study not only maximum mass configurations but also three stars with masses $1\,M_{\odot}$, $1.44\,M_{\odot}$ and $1.67\,M_{\odot}$. Any of these observed stars have a central density that goes from 1.14 ρ_0 to 1.82 ρ_0 within the framework of our model, and therefore we will be testing the equation of state at supra-saturation densities. As a first approximation we will discuss only neutron stars constituted only by neutrons, protons, electrons and muons. At high density the formation of hyperons is energetically favourable and the effect of the symmetry energy on the appearance of these exotic degrees of freedom [5,10] is important to neutron star structure, therefore we introduce the full Lagrangian density including hyperons and calculate some consequences for star structure. This will be considered in more detail in future work. In section 1.2 we make a small description of how neutron stars may appear. We start by making a presentation of the main aspects of relativistic mean field theory in chapter 2. In chapter 3 we make a short discussion on what is needed to know the structure of a neutron star and content. In chapter 4 we develop the formalism and discuss the results. In chapter 5 some conclusions are drawn.

1.2 A sketch of stellar evolution

The interstellar medium (ISM) is very tenuously composed of gases and dust. The average density of the ISM is approximately one atom per cubic centimetre and represents ≈20-30% of the mass of a galaxy. The interstellar dust particles have a medium size of approximately 450 - 495 nm and are composed mostly of hydrogen (H), carbon (C), oxygen (O), silicon (Si), magnesium (Mg) and iron (Fe) in the form of silicates, graphite, ices, metals and organic compounds. Nebulae are denser agglomerations of gas and dust that may coexist with newly born or dead stars. Huge complexes of interstellar gas and dust left over from the formation of galaxies, called *molecular clouds* (MC), are composed mostly of molecular hydrogen. They are the densest (10^6 particles/cm^3) and coolest (10 to 20 K) objects. Their size ranges over 1 light-year to 300 light-years and have the possibility of forming 10 to 10^7 stars like our Sun. MC's that exceed a mass of about 10^5 solar masses are called *giant molecular clouds* (GMC). In a common spiral galaxy there are a 1000 to 2000 of these objects and many other smaller ones. Because these clouds do not emit visible light, they emit mostly radio waves, they were first discovered in our own Milky Way galaxy by radio telescopes. There is a GMC in the Orion constellation that was mapped by its carbon monoxide content. Star forming GMC's are found mostly in the arms of spiral galaxies. GMC's are internally violent and turbulent, the self gravitational energy of clumps of matter is counter balanced by the pressure from the gases and magnetic field lines. Perturbations from the spiral density within the spiral arm, collisions with other parts of the GMC, supernova shock-waves and closeby massive star formation make up for some of the triggers that cause the necessary imbalance within the GMC for the clumps of matter to begin collapsing. As a gas core begins collapsing it heats up due to friction of its constituents. The gravitational energy of the gas particles gets converted into thermal energy. The gas cores become warm enough to produce infrared and microwave radiation. The initial collapse is very quick and as the core becomes more and more dense it becomes more and more opaque to radiation. The radiation gets trapped inside the core and the temperature and pressure in the centre begins to increase. The core starts evolving into a proto-star, it has only 1% of its final mass and it continues to grow because of gravity. After some millions of years the temperature at the centre of the core becomes hot enough to fuse hydrogen. This prevents further accretion because of the strong stellar wind it causes. Proto-stars reach temperatures of 2000 to 3000 K, hot enough to send red light but they are enveloped in gas and dust that blocks visible light from escaping. The transition from proto-stars to stars is not assured, in fact, only 10% of all proto-stars survive the savage formation regions to become stars and planetary systems.

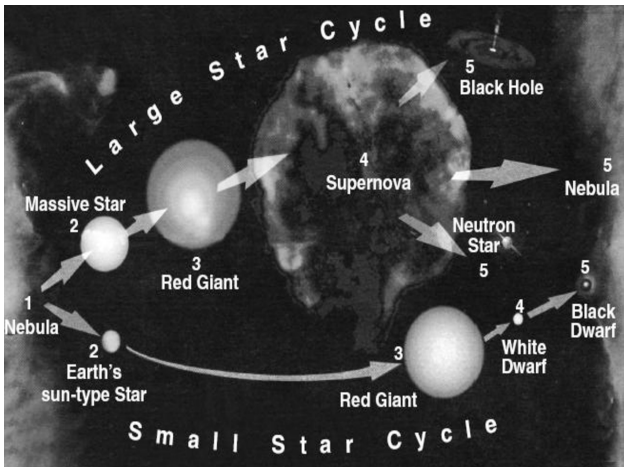

Figure 1.1: Scheme of stellar evolution. Source: Chandra X-Ray observatory.

If the mass of the star is high enough (≈8 to 30$M_\odot$) in its final stage just before becoming a supernova it will turn out being a very compact neutron star (average density $\approx 7 \times 10^{14}$ g/cm^3) with a radius of approximately 10-15 km and $\approx 1.4M_\odot$ (Chandrasekhar mass). One other way, maybe, of forming neutron stars is to have a white dwarf accrete enough mass to reach the Chandrasekhar mass, causing a collapse but this is a speculation. In the 10 billion year lifetime of the galaxy there have probably been 10^8 to 10^9 neutron stars formed in favour of the formation of black holes which is harder to accomplish. In figure 1.1 we have a schematic notion of how black holes, neutron stars and dwarfs stars are formed. Astronomers can find black holes and neutron stars by observing the effects on other objects nearby. The intense gravity from a black hole or a neutron star will pull in dust particles from a surrounding cloud of dust or a nearby star and as the particles speed up and heat up, they emit x-rays. They can also be detected by observing rapidly rotating stars around an x-ray source. If neutron stars or black holes are alone in space we can infer their presence by gravitational lensing. Compact stars are a playground in which we can test and extend our knowledge of the atomic nucleus. They are a glimpse at the amazing structures brought about by the hitherto earthly non replicable conditions of the cosmos and also provides us new sorts of tests for general relativity.

Chapter 2

RELATIVISTIC NUCLEAR MEAN FIELD THEORY

2.1 Nuclear properties

Of all the densities found on a neutron star, at some point, we should find the usual nuclear density that we find in our common experiments. The theory that we use to describe nuclei is also used to describe neutron stars. Our current knowledge of the nucleus was much clarified in the years that passed since the Rutherford experiment and now correlates thousands of data with a precision higher than was ever achieved. We characterize the nuclei binding energy by its mass number (A), proton (Z) and neutron (N) numbers. Nuclei are saturated systems because the strong force that binds nucleons is short ranged and it is repulsive at very short distances. This means that the density of the central region remains constant, even if we add more nucleons to nuclei. Nuclei with neutron number N close to proton number Z are more tightly bound than their neighbour nuclei and even numbers for both N and Z are more likely. The latter property reflects to some extent the Pauli principle. Nucleons in the interior of nuclei are more bound because they are completely surrounded by other attracting nucleons and the nucleons on the surface will have a smaller number of nucleons binding them[1]. Let's consider the nuclear mass $m(Z, A)$. Any nucleus can, in principle, be pulled apart into Z protons and $N = A - Z$ neutrons. If the nucleus is stable against break-up into individual nucleons, its mass $m(Z, A)$ should be smaller than the sum of the individual masses of the protons and neutrons when separated by large distances that is

$$m(Z, A) = Zm_p + Nm_n - B \tag{2.1.1}$$

m_n and m_p are the masses of the neutron and the proton respectively and B is the nuclear binding energy. B is the energy required to dismantle the nucleus into Z protons and N neutrons. In the nuclear liquid drop model we write the binding energy per nucleon ($\frac{B}{A}$) for a nucleus in the

[1] If the nucleus is very large they will have at best, on average, half the number of nucleons of a nucleon on the interior binding them.

form

$$\frac{B}{A}(A,Z) = a_{\text{volume}} - a_{\text{symmetry}}\left(\frac{Z-N}{A}\right)^2 - a_{\text{surface}}A^{-1/3} - a_{\text{coulomb}}Z(Z-1)A^{-4/3} + \\ + \frac{(-1)^N + (-1)^Z}{2}\frac{a_{\text{pairing}}}{\sqrt{A}} + \ldots \quad (2.1.2)$$

This is the Weizsäcker formula, $B(A,Z)$ is a truncated power series in A for a certain nucleus with mostly non-integer negative exponents. We can adjust the resulting curve to experimental data, one of such fits leads to $a_{\text{volume}} = 15.75$, $a_{\text{symmetry}} = 23.7$, $a_{\text{surface}} = 17.8$, $a_{\text{coulomb}} = 0.710$ and $a_{\text{pairing}} = 34.0$ all in MeV. In the limit $A \to \infty$ and picturing nuclear matter as a degenerate Fermi gas we get, from another fit:

$$\rho_0 = 0.153 \text{ fm}^{-3} \quad (2.1.3a)$$

$$\frac{B}{A} = -16.3 \text{ MeV} \quad (2.1.3b)$$

$$a_{sym} = 32.5 \text{ MeV} \quad (2.1.3c)$$

Experimental evidence also allows us to extrapolate the ranges in which the Dirac effective mass m_N^* and the incompressibility ($\mathcal{K}$) should be:

$$0.7 < m_N^*/m_N < 0.8 \text{ (Dirac nucleon effective mass/nucleon mass)} \quad (2.1.4a)$$

$$230.0 < \mathcal{K} < 250.0 \text{ MeV (compression modulus)} \quad (2.1.4b)$$

2.2 Nonlinear Walecka model

Experimental measurements of electron scattering from high-momentum nucleons in nuclei allows one to conclude that in normal nuclear matter approximately 25% of the nucleons have one quarter of the speed of light [11] which means that we need to use special relativity to describe nuclei, thus we must make our theory Lorentz covariant. It also has to be quantum mechanically consistent because we are dealing with very small distances ≈ 1 fm. In this section we will see first in broad terms how Johnson and Teller [12], Duerr [13] and Walecka [14] developed a renormalised quantum field theory (σ-ω model) for the description of nuclei and based it on the locally Lorentz invariant fields of four types of particles: the nucleons and two mesons; a scalar meson σ and a iso-scalar-vector meson ω both responsible for the coupling between nucleons. It is observed that nuclear forces are repulsive at very short range (≈ 0.3 fm) and are attractive at greater distances (up to ≈ 1.5 fm). One effective potential that approximately describes the force between nucleons is given by

$$V_{\sigma\omega}(r) = \frac{g_\omega^2}{4\pi}\frac{e^{-m_\omega r}}{r} - \frac{g_\sigma^2}{4\pi}\frac{e^{-m_\sigma r}}{r} \quad (2.2.1)$$

where g_σ, g_ω, m_σ and m_ω are the coupling constants and the masses of the neutral σ and ω mesons (see table 2.1) and r is the relative distance between nucleons. Each of the terms $\frac{g_\omega^2}{4\pi}\frac{e^{-m_\omega r}}{r}$ and $\frac{g_\sigma^2}{4\pi}\frac{e^{-m_\sigma r}}{r}$ are Yukawa like potentials. In $V_{\sigma\omega}(r)$ σ is stronger than ω for intermediate separations and weaker than ω for short distances, we can see this in figure 2.1. For the baryons,

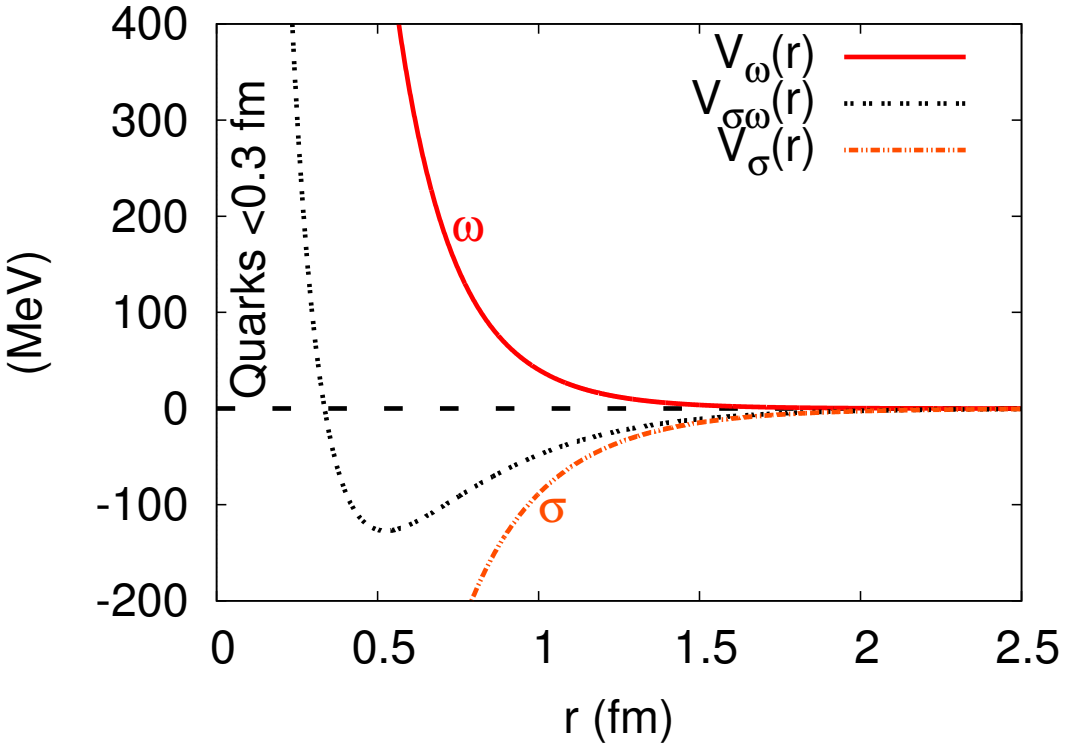

Figure 2.1: Effective nuclear potential versus inter-nucleon distance r in the σ-ω model illustrating short-range repulsion and intermediate-range attraction.

since they are Fermions we use the Dirac Lagrangian density with ψ as their field and m as their mass. The σ meson is represented with the Klein-Gordon Lagrangian density with a mass m_σ. The ω meson can be represented by the Proca Lagrangian density with mass m_ω. The full Lagrangian density is the sum of all these three components and the interactions $g_\sigma\bar{\psi}\sigma\psi$, $g_\omega\bar{\psi}\gamma_\mu\omega^\mu\psi$

$$\begin{aligned}\mathcal{L}_W = \bar{\psi}\left[\gamma_\mu\left(i\partial^\mu - g_\omega\omega^\mu\right) - \left(m - g_\sigma\sigma\right)\right]\psi + \\ \frac{1}{2}\left(\partial_\mu\sigma\partial^\mu\sigma - m_\sigma^2\sigma^2\right) - \frac{1}{4}\Omega_{\mu\nu}\Omega^{\mu\nu} + \frac{1}{2}m_\omega^2\omega_\mu\omega^\mu\end{aligned} \tag{2.2.2}$$

with $\Omega_{\mu\nu} = \partial_\mu\omega_\nu - \partial_\nu\omega_\mu$ and where g_σ and g_ω are coupling constants to be defined according to table 2.1, the quantum-hadro-dynamics I (**QHD-I**) [15] parameter set. Please note that here we use the same greek letter to denote the meson and the field, σ. These fields and couplings provide the smoothest average nuclear interactions and this way are best to describe bulk nuclear matter. This simple Lagrangian allows one to reproduce two things, the saturation density

	m (MeV)	m_σ (MeV)	m_ω (MeV)	g_σ	g_ω
QHD-I	939	550	783	9.57	11.67

Table 2.1: σ-ω model parameter set.

ρ_0 (fm^{-3})	$\mathcal{K}$ (MeV)	m^*/m	-B/A (MeV)	a_{sym} (MeV)	L (MeV)
0.193	540	0.556	16.3	22.1	74.3

Table 2.2: σ-ω model saturation properties with the QHD-I parameter set.

$\rho_0 = 0.193$ fm^{-3} and the binding energy at saturation $B/A = -16.3$ MeV. Other properties are not well reproduced, the symmetry energy is too low (22.1 MeV) and the incompressibility is too high (540 MeV). From the Euler-Lagrange equations

$$\partial_\alpha \left(\frac{\partial \mathcal{L}}{\partial(\partial_\alpha \phi_\beta)} \right) = \frac{\partial \mathcal{L}}{\partial \phi_\beta} \tag{2.2.3}$$

we get the equations of motion

$$\left\{ \gamma_\mu \left(i\partial^\mu - g_\omega \omega^\mu \right) - m^* \right\} \psi = 0 \tag{2.2.4a}$$

$$\left(\partial_\mu \partial^\mu + m_\sigma^2 \right) \sigma = g_\sigma \bar{\psi} \psi \tag{2.2.4b}$$

$$\partial_\mu \Omega^{\mu\nu} + m_\omega^2 \omega^\nu = g_\omega \bar{\psi} \gamma^\nu \psi \tag{2.2.4c}$$

Equation (2.2.4a) is the Dirac equation for the nucleons with $m^* = m - g_\sigma \sigma$ as the effective mass. Equation (2.2.4b) is the Klein-Gordon equation for the σ meson with a scalar perturbation from the Dirac baryon fields. Equation (2.2.4c) is very similar to the quantum electrodynamics Proca equation except the current is now baryonic, $g_\omega \bar{\psi} \gamma^\nu \psi$. Using the energy momentum tensor definition

$$T^{\mu\nu} = \frac{\partial \mathcal{L}}{\partial(\partial_\mu \phi_\beta)} \partial^\nu \phi_\beta - g^{\mu\nu} \mathcal{L} \tag{2.2.5}$$

we get

$$\begin{aligned} T_{\mu\nu} = \frac{1}{2} \Bigg[-\partial_\lambda \sigma \partial^\lambda \sigma + m_\sigma^2 \sigma^2 + \frac{1}{2} \Omega_{\lambda\delta} \Omega^{\lambda\delta} - m_\omega^2 \omega_\lambda \omega^\lambda \Bigg] g_{\mu\nu} \\ + i\bar{\psi} \gamma_\mu \partial_\nu \psi + \partial_\mu \sigma \partial^\nu \sigma + \partial_\nu \omega^\lambda F_{\lambda\mu} \end{aligned} \tag{2.2.6}$$

Our purpose is to study bulk nuclear matter, and in this case the right hand sides of equations (2.2.4b) and (2.2.4c) get very large as the nucleon density increases so we can replace the values of the fields for their expectation values

$$\sigma(x) \to \langle \sigma(x) \rangle = \sigma_0 = \sigma \tag{2.2.7a}$$

$$\omega_\mu(x) \to \langle \omega_\mu(x) \rangle = \delta_{\mu 0} \omega_0 = \omega \tag{2.2.7b}$$

This is the *mean field approximation* (MFA). Now we transform equations (2.2.4b) and (2.2.4c) into

$$m_\sigma^2 \sigma = g_\sigma \langle \bar{\psi}\psi \rangle \tag{2.2.8a}$$

$$m_\omega^2 \omega = g_\omega \langle \bar{\psi}\gamma^0\psi \rangle \tag{2.2.8b}$$

Casting it into a computationally tractable form, we get

$$g_\sigma \sigma = \left(\frac{g_\sigma}{m_\sigma}\right)^2 \frac{1}{\pi^2} \int_0^{k_F} k^2 \frac{m - g_\sigma\sigma}{\sqrt{k^2 + (m - g_\sigma\sigma)^2}} dk \tag{2.2.9a}$$

$$g_\omega \omega = \left(\frac{g_\omega}{m_\omega}\right)^2 \rho \tag{2.2.9b}$$

From the energy momentum tensor, we get the energy density and the pressure[2]:

$$\varepsilon = -\langle \mathcal{L} \rangle + \langle \bar{\psi}\gamma_0 k_0 \psi \rangle \tag{2.2.10a}$$

$$p = \langle \mathcal{L} \rangle + \frac{1}{3}\langle \bar{\psi}\gamma_i k_i \psi \rangle \tag{2.2.10b}$$

which transforms into

$$\varepsilon = \frac{1}{2}m_\sigma^2\sigma^2 + \frac{1}{2}m_\omega^2\omega^2 + \frac{\gamma}{2\pi^2}\int_0^{k_F} k^2 \sqrt{k^2 + (m - g_\sigma\sigma)^2}\, dk \tag{2.2.11a}$$

$$p = -\frac{1}{2}m_\sigma^2\sigma^2 + \frac{1}{2}m_\omega^2\omega^2 + \frac{1}{3}\frac{\gamma}{2\pi^2}\int_0^{k_F} \frac{k^4}{\sqrt{k^2 + (m - g_\sigma\sigma)^2}}\, dk, \tag{2.2.11b}$$

where γ is the degeneracy of the baryons. In this work all plots pertaining to the σ-ω model it was used $\gamma = 4$ (symmetric nuclear matter), i.e. an equal fraction of protons and neutrons. The expression for the pressure was found using the energy-momentum tensor but we could use thermodynamic definition

$$p = -\frac{\partial E}{\partial V} \tag{2.2.12}$$

by dividing E and V by the total number of particles, N, getting

$$p = \rho^2 \frac{\partial}{\partial \rho}\left(\frac{\varepsilon}{\rho}\right) \tag{2.2.13}$$

It's possible to use (2.2.13) to get (2.2.11b) in this case or in any other that we will discuss in this work. Having the equations (2.2.11a) and (2.2.9a) we can now calculate all the properties of nuclear matter (2.1.3). The effective mass $m^* = m - g_\sigma\sigma$ is the reduced baryon mass by the

[2]Which we can cast into an equation of state $p(\varepsilon)$.

interaction of the σ field with the baryons ψ. It tends to zero at high densities. The binding energy can be calculated by comparison of (2.1.2) with (2.2.11a) by introducing[3]

$$\frac{B}{A} = \frac{\varepsilon}{\rho} - m \tag{2.2.14}$$

The symmetry energy can be obtained by comparison of (2.2.10a) with (2.1.2)

$$a_{sym} = \frac{1}{2}\left[\left(\frac{\partial^2 (\varepsilon/\rho)}{\partial t^2}\right)\right]_{t=0} \tag{2.2.15}$$

with $t = \frac{\rho_n - \rho_p}{\rho}$ and $\rho = \rho_n + \rho_p$, a_{sym} is then calculated to be

$$a_{sym} = \frac{k_F^2}{6\sqrt{k_F^2 + (m - g_\sigma \sigma)^2}} \tag{2.2.16}$$

This function corresponds to the coefficient a_{sym} in formula (2.1.2), the higher it gets the lower will be the binding energy if we have asymmetry ($N \neq Z$). The slope L of the symmetry energy is defined as

$$L = 3\rho_0 \frac{da_{sym}}{d\rho}\bigg|_{\rho=\rho_0} \tag{2.2.17}$$

and indicates how fast will a_{sym} grow with density. We can get the incompressibility from the formula:

$$\mathcal{K} = 9\left[\rho^2 \frac{\partial^2}{\partial \rho^2}\left(\frac{\varepsilon}{\rho}\right)\right]_{\rho=\rho_0} \tag{2.2.18}$$

The incompressibility, $\mathcal{K}$, gives us the information of how fast the EOS rises with density. The larger $\mathcal{K}$ is the faster the EOS rises and the harder it gets to compress nuclear matter. The σ-ω model of nuclear matter has, at best, only two properties that are very close to the phenomenological value $\frac{B}{A} \approx -15.75$ MeV and $\rho_0 = 0.193$ fm^{-3}. All the other variables are in disparity from what is desired, namely $m^*/m \approx 0.5$ which is too low, the too high value of the incompressibility $\mathcal{K} = 540$ MeV and the symmetry energy of 22.1 MeV is below the expected value of ≈ 33 MeV. The slope of the symmetry energy is 74.3 MeV which is acceptable within the parameter sets mentioned in [8] and still is under investigation. This way the Walecka model is a good starting point on the study of nuclear matter and further study has shown that it can be perfected. Boguta and Bodmer [16] extended the theory further by adding self-interactions of the scalar field to the Lagrangian density (2.2.2)

$$U(\sigma) = \frac{\kappa}{3!}\sigma^3 + \frac{\lambda}{4!}\sigma^4 \tag{2.2.19}$$

where $\kappa = 2mg_\sigma^3 b$ and $\lambda = 6g_\sigma^4 c$ are coupling constants (see table 2.4). The introduction of these nonlinear σ allow a better adjustment to the incompressibility $\mathcal{K}$ and the effective mass, m^* (see

[3]Note that we can now write $p = \rho^2 \frac{\partial}{\partial \rho}\left(\frac{B}{A}\right)$

table 2.5). Besides the phenomenological need of these terms, there is also a theoretical reason for their presence, the model becomes renormalizable. One of the consequences of renormalization is that once the parameters of the model are selected to fit observed nuclear properties, we can extrapolate into regimes of high density or temperature whithout the appearance of new unknown sets of parameters. The equations of motion for the new Lagrangian density $\mathcal{L}_W - U(\sigma)$ are the same as (2.2.4a) except for the σ equation (2.2.4b) which transforms into

$$\left(\partial_\mu \partial^\mu + m_\sigma^2\right)\sigma = g_\sigma \bar{\psi}\psi - \frac{\kappa}{2}\sigma^2 + \frac{\lambda}{3!}\sigma^3 \tag{2.2.20}$$

introducing a correction in the baryon effective mass. The equation of state also changes:

$$\varepsilon = \frac{\kappa}{3!}\sigma^3 + \frac{\lambda}{4!}\sigma^4 + \frac{1}{2}m_\sigma^2\sigma^2 + \frac{1}{2}m_\omega^2\omega^2 + \frac{\gamma}{2\pi^2}\int_0^{k_F} k^2\sqrt{k^2 + (m - g_\sigma\sigma)^2}\, dk \tag{2.2.21a}$$

$$p = -\frac{\kappa}{3!}\sigma^3 - \frac{\lambda}{4!}\sigma^4 - \frac{1}{2}m_\sigma^2\sigma^2 + \frac{1}{2}m_\omega^2\omega^2 + \frac{1}{3}\frac{\gamma}{2\pi^2}\int_0^{k_F} \frac{k^4}{\sqrt{k^2 + (m - g_\sigma\sigma)^2}}\, dk \tag{2.2.21b}$$

Further development is possible by adding the nonlinear ω^μ term

$$U(\omega^\mu) = \frac{\xi}{4!}g_\omega^4(\omega_\mu\omega^\mu)^2, \tag{2.2.22}$$

where ξ is a coupling constant, which allows corrections of the symmetry energy in high densities (see tables 2.4 and 2.5). To be able to alter the proton fraction ($Y_p = \frac{\rho_p}{\rho_p + \rho_n}$) we add the terms for the vector-isovector $\vec{\rho}^{\,\mu}$ meson to also include isospin

$$U(\vec{\rho}^{\,\mu}) = -i\bar{\psi}\gamma_\mu\frac{g_\rho}{2}\vec{\tau}\cdot\vec{\rho}^{\,\mu}\psi - \frac{1}{4}\vec{R}_{\mu\nu}\cdot\vec{R}^{\mu\nu} + \frac{1}{2}m_\rho^2\vec{\rho}_\mu\cdot\vec{\rho}^{\,\mu} \tag{2.2.23}$$

with $\vec{R}_{\mu\nu} = \partial_\mu\vec{\rho}_\nu - \partial_\nu\vec{\rho}_\mu - g_\rho\vec{\rho}_\mu\times\vec{\rho}_\nu$, $\vec{\tau}$ is the isospin operator, g_ρ is a coupling constant and m_ρ is the ρ meson mass (see tables 2.4 and 2.5). The total nonlinear Walecka model (NLWM) Lagrangian density is then defined as

$$\begin{aligned}\mathcal{L}_{NLWM} = \bar{\psi}\left[\gamma_\mu\left(i\partial^\mu - g_\omega\omega^\mu - \frac{g_\rho}{2}\vec{\tau}\cdot\vec{\rho}^{\,\mu}\right) - (m - g_\sigma\sigma)\right]\psi + \\ + \frac{1}{2}\partial_\mu\sigma\partial^\mu\sigma - \frac{1}{2}m_\sigma^2\sigma^2 - \frac{\kappa}{3!}\sigma^3 - \frac{\lambda}{4!}\sigma^4 + \\ - \frac{1}{4}\Omega_{\mu\nu}\Omega^{\mu\nu} + \frac{1}{2}m_\omega^2\omega_\mu\omega^\mu + \frac{\xi}{4!}g_\omega^4\left(\omega_\mu\omega^\mu\right)^2 + \\ - \frac{1}{4}\vec{R}_{\mu\nu}\cdot\vec{R}^{\mu\nu} + \frac{1}{2}m_\rho^2\vec{\rho}_\mu\cdot\vec{\rho}^{\,\mu}\end{aligned} \tag{2.2.24}$$

Table 2.3 lists some of the properties of all the mesons used in the NLWM lagrangian density. Note that the same letter was attributed to the σ meson as to the field σ. After the MFA the equations of motion become

$$0 = g_\sigma \langle \bar{\psi}\psi \rangle - m_\sigma^2 \sigma - \frac{\kappa}{2}\sigma^2 - \frac{\lambda}{3!}\sigma^3 \tag{2.2.25a}$$

$$0 = g_\omega \langle \bar{\psi}\gamma^0\psi \rangle - m_\omega^2 \omega - \frac{\xi}{3!}\omega^3 \tag{2.2.25b}$$

$$m_\rho^2 \rho_{03} = \frac{g_\rho}{2} \langle \bar{\psi}\gamma_0\tau_3\psi \rangle \tag{2.2.25c}$$

The first of these equations for NLWM (2.2.25a) and for σ-ω, equation (2.2.9a) allows us to define the effective mass for both models. The parameter set TM1 was determined as the best

Meson	m (MeV)	Quark content	Spin	Isospin	Charge	τ (s)
σ	550	-	0	0	-	-
ω	783	$u\bar{u} + d\bar{d}$	1	0	-	7×10^{-23}
ρ	770	$u\bar{d}, d\bar{u}, (u\bar{u} - d\bar{d})/2$	1	1	(+1,0,-1)	0.36×10^{-23}

Table 2.3: Mesons that represent the interactions of the NLWM model, their masses, quark content, spin, isospin, electric charge (in units of e^-) and lifetimes (in seconds).

to reproduce the properties of nuclei [19], even unstable ones are included. The fit of TM1 to nuclear matter is in very good agreement with experimental data.

m_σ (MeV)	m_ω (MeV)	m_ρ (MeV)	g_σ	g_ω	g_ρ	b	c	ξ
511.19	783	770	10.029	12.614	9.264	0.00156	0.000061	0.0169

Table 2.4: NLWM model **TM1** [19] parameter set. The nucleon mass is $m = 938$ MeV.

ρ_0 (fm^{-3})	$\mathcal{K}$ (MeV)	m^*/m	-B/A (MeV)	a_{sym} (MeV)	L (MeV)
0.145	281	0.634	16.29	36.8	110.7

Table 2.5: NLWM model TM1 saturation properties.

We can see in figure 2.2 how the NLWM model for nuclear matter improves on the σ-ω model effective mass by rising it from 0.556 to 0.6 at saturation density.

The EOS changes:

$$\varepsilon = \frac{\kappa}{3!}\sigma^3 + \frac{\lambda}{4!}\sigma^4 + \frac{1}{2}m_\sigma^2\sigma^2 + \frac{1}{2}m_\omega^2\omega^2 + \frac{\xi}{6!}(g_\omega\omega)^4 + \frac{1}{2}m_\rho^2\rho_{03}^2 + \frac{1}{\pi^2}\sum_{i=1}^{2}\int_0^{k_{Fi}} k^2\sqrt{k^2 + (m - g_\sigma\sigma)^2}\, dk \tag{2.2.26}$$

$$p = -\frac{\kappa}{3!}\sigma^3 - \frac{\lambda}{4!}\sigma^4 - \frac{1}{2}m_\sigma^2\sigma^2 + \frac{1}{2}m_\omega^2\omega^2 + \frac{\xi}{6!}(g_\omega\omega)^4 + \frac{1}{2}m_\rho^2\rho_{03}^2 + \frac{1}{3}\frac{1}{\pi^2}\sum_{i=1}^{2}\int_0^{k_{Fi}} \frac{k^4}{\sqrt{k^2 + (m - g_\sigma\sigma)^2}}\, dk \tag{2.2.27}$$

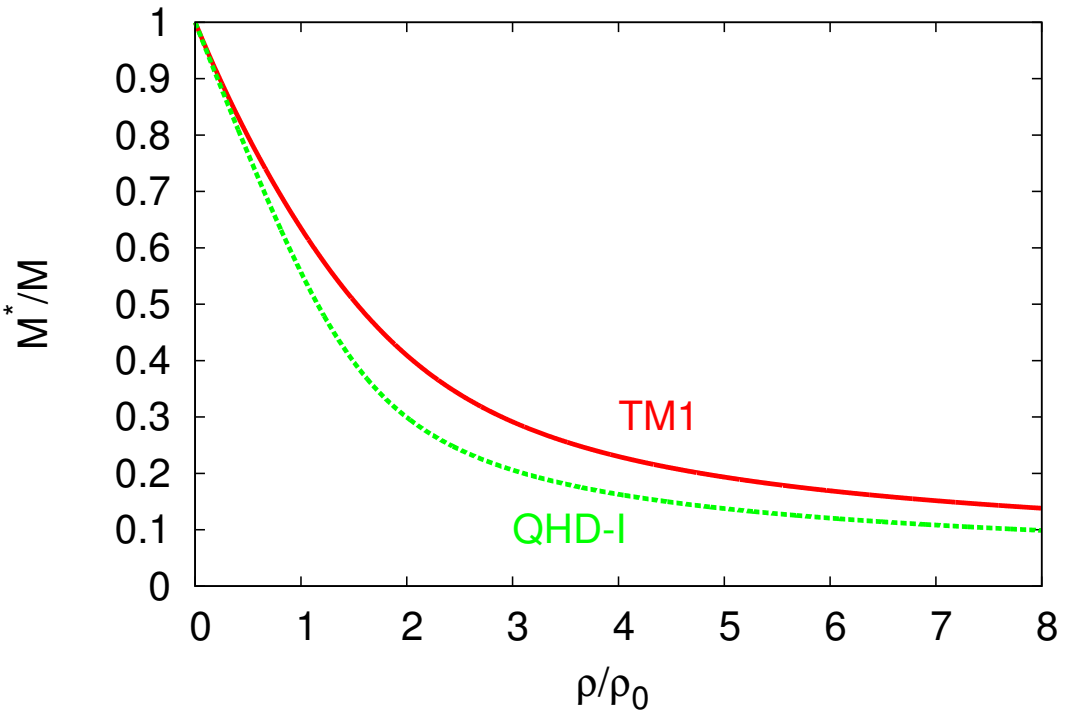

Figure 2.2: Effective mass versus density in the σ-ω and in the NLWM models of nuclear matter for the QHD-I and the TM1 parameter sets respectively.

The sum in both equations is on neutron and proton Fermi momentum. The symmetry energy has now a different form

$$a_{sym} = \left(\frac{g_\rho}{m_\rho}\right)^2 \frac{k_F^3}{12\pi^2} + \frac{k_F^2}{6\sqrt{k_F^2 + m^{*2}}} \tag{2.2.28}$$

and figure 2.3 lets us see the change made by NLWM in comparison with the σ-ω model. The symmetry energy now has a higher value at saturation density ($a_{sym} = 36.8$ MeV) than the value obtained by σ-ω ($a_{sym} = 22.1$ MeV) bringing the symmetry energy closer to the requirement in (2.1.3c). In figure 2.4 the slope of the symmetry energy is plotted for the two models σ-ω and NLWM. The NLWM model rises the value of the slope at saturation density from $L = 74.3$ MeV to $L = 110.7$ MeV. Both are in accordance with some phenomenological extrapolations [17, 18]. The curves for the binding energy per nucleon in either of the models are fitted to the saturation properties (see figure 2.5) $B/A \approx -16.3$ MeV and the saturation density is almost the same for the two models. The difference in the incompressibility in the two models σ-ω is clear in figure 2.5 because B/A rises so much faster in σ-ω ($\mathcal{K} = 540$ MeV) than B/A for NLWM ($\mathcal{K} = 281$ MeV). This also means that nuclear matter is more bound for high densities in NLWM than in σ-ω.

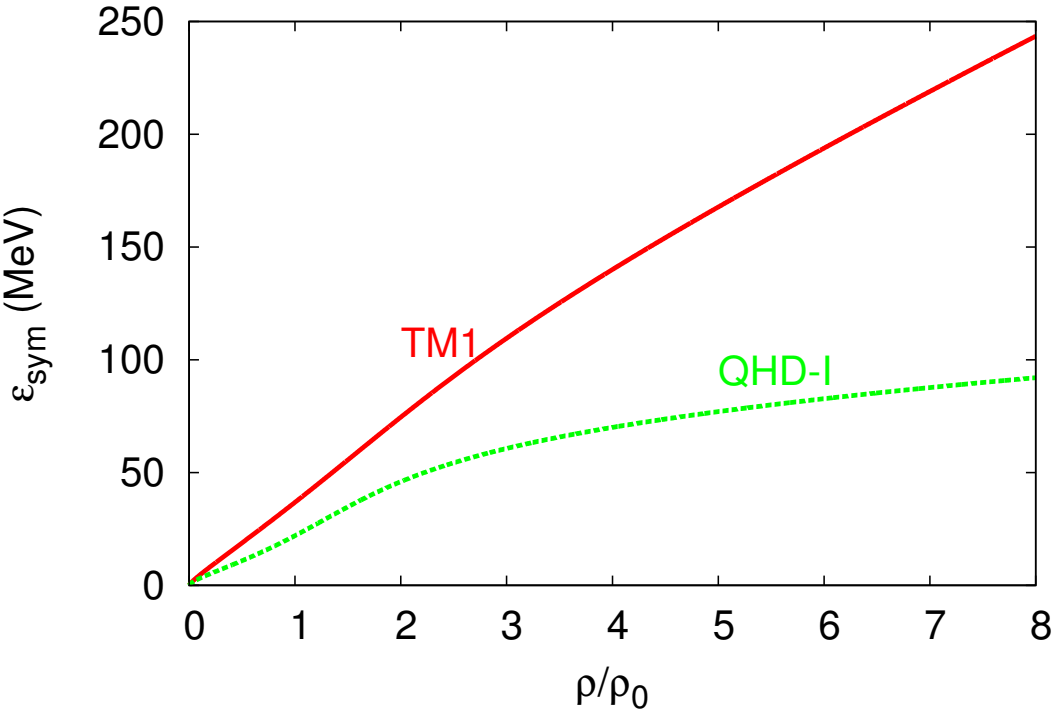

Figure 2.3: Symmetry energy versus density in the Walecka σ-ω and in the NLWM models with the QHD-I and TM1 parameter sets respectively.

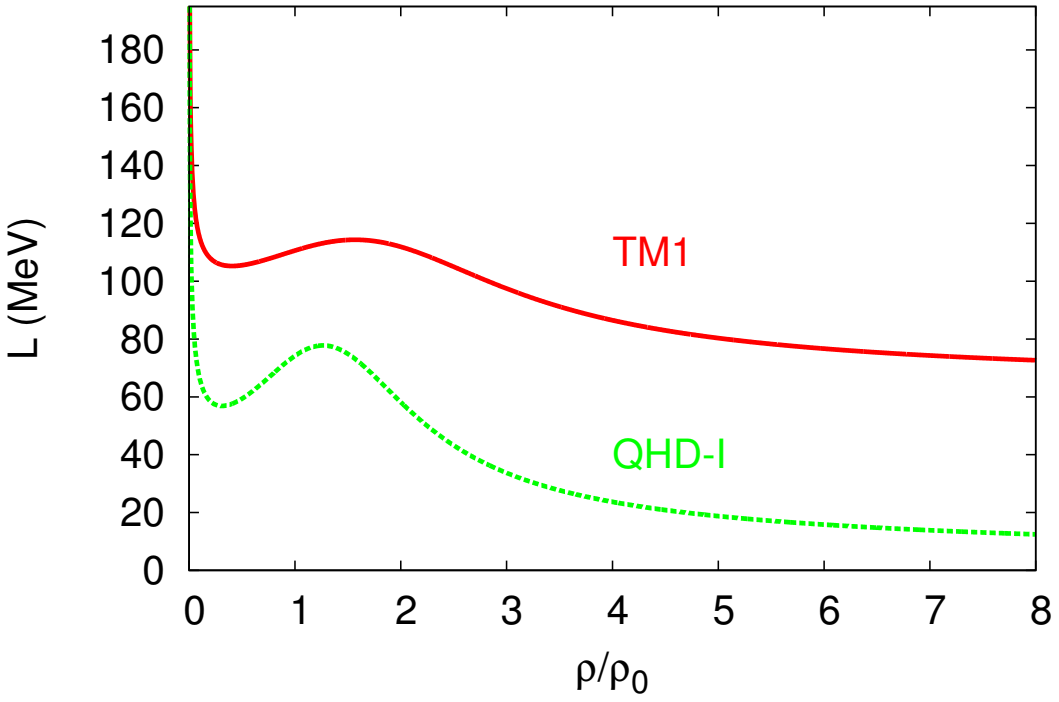

Figure 2.4: The slope of the symmetry energy as a function of density in the σ-ω (QHD-I parameter set) and in the NLWM (TM1 parameter set) models of nuclear matter.

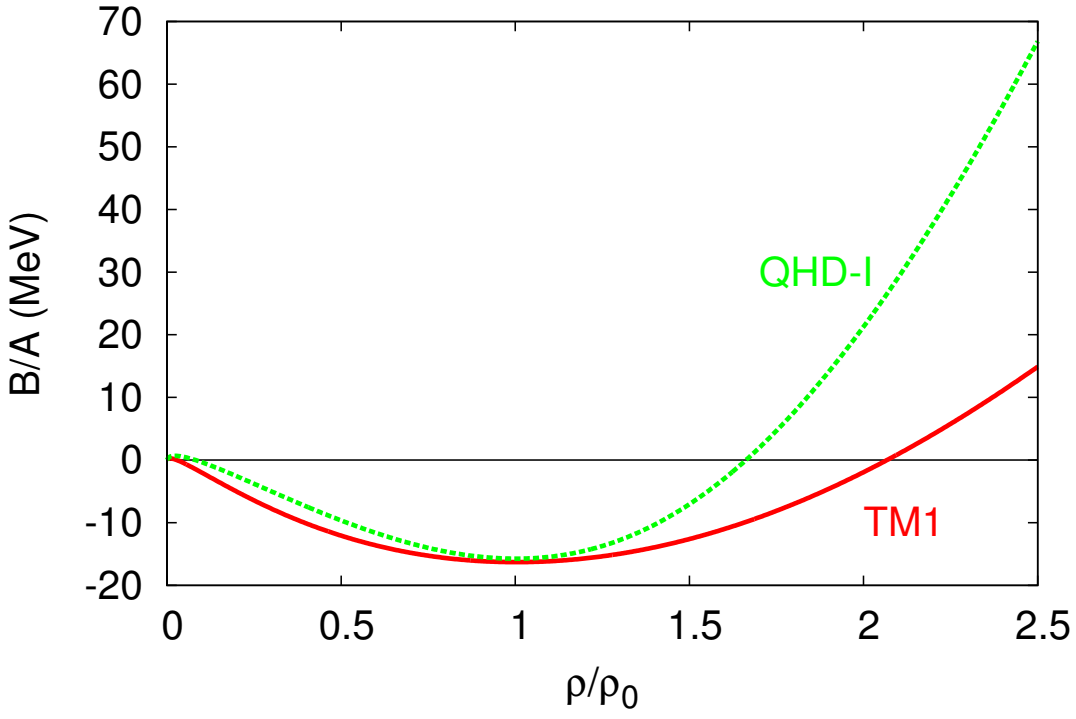

Figure 2.5: The binding energy per nucleon as a function of density in the σ-ω and in the NLWM models of nuclear matter with the parameter sets indicated in the figure.

Chapter 3

COLD NEUTRON STARS

3.1 Tolmann-Oppenheimer-Volkov equations

To describe such a dense object as a neutron star we must use general relativity (GR). In this work we consider a neutron star to be a spherically symmetric, homogeneous, isotropic and static mass agglomeration. The GR prescription to calculate its properties is the Tolmann-Oppenheimer-Volkov (TOV) pair of equations, to be solved simultaneously

$$M(r) = 4\pi \int_0^r \varepsilon(r) r^2 dr \tag{3.1.1a}$$

$$\frac{dp}{dr}(r) = -\frac{p(r) + \varepsilon(r)}{r\left[r - 2M(r)\right]} \left\{M(r) + 4\pi r^3 p(r)\right\} \tag{3.1.1b}$$

where ε is the energy density, p is the pressure, $M(r)$ is the total mass of the star up to radius r. We solve the equations simultaneously from the origin ($r = 0$) out, subject to the boundary conditions

$$p(r = R) = 0 \tag{3.1.2a}$$

$$M(0) = 0 \tag{3.1.2b}$$

$p(r = R) = 0$ means that at some point r in the calculation we force $p = 0$ and at that point we will define the $r = R$ radius of the star. At the same time we will define $M(R)$ the total mass of the star. The energy density and the pressure we use as input depends on the constituent matter of the star we want to build. In our case, we will make it of nuclear matter. For each EOS there is a different central energy density $\varepsilon(0) = \varepsilon_c$ and central pressure $p(0) = p_c$. Each EOS defines a unique relation between $[r, \varepsilon(r), p(r), \rho(r), M(r)]$ and also maximum mass and radius.

3.2 Nuclear and neutron star matter

Neutron stars have masses $M \approx 1 - 2M_{\odot}$ and radii $R \approx 10 - 12$ km [20]. The main similarity of nuclei and neutron stars is that both contain nucleons and at some point along its radius, the neutron star has a density equal to the normal nuclear density. Neutron stars are bound by the long range gravitational force and nuclei by the short ranged nuclear strong force. The gravitational force acts on everything that is mass or energy. The normal nuclear matter density is $\rho_0 = 2.8 \times 10^{14}$ g cm^{-3} and the average densities inside a neutron star are

$$\bar{\rho} = \frac{3M}{4\pi R^3} = 7 \times 10^{14} \text{ g cm}^{-3} \approx (2-3)\rho_0 \tag{3.2.1}$$

and in the centre it is much larger, of the order $\approx (5-10)\rho_0$. On the other hand, nucleons inside a neutron star, feel repulsion because of being so tightly packed together. In this way the nuclear force contributes negatively to the binding energy of a neutron star. The binding energy per nucleon due to gravity in a neutron star is ≈ 160 MeV/A and inside a nucleus, mostly due to the nuclear force, is ≈ 16 MeV/A [10, 20]. The charge in a nucleus is positive and the charge density changes significantly with total baryon density as we can see in figure 3.1 where we plot the more stable nuclei neutron number as a function of proton number. The total number of charged particles inside a neutron star Z_{net}, is virtually zero. Let us try to build a spherical star of radius R that is composed of same charge particles but bound by gravity. We should then force the condition that the electrical force that pulls them apart should be smaller than the gravitational force that pulls them inside[1], i.e.

$$\begin{aligned} ||\vec{F}_e|| < ||\vec{F}_g|| \Leftrightarrow K_e \frac{(Z_{net}e)e}{R^2} < G\frac{(Am)m}{R^2} \Leftrightarrow Z_{net} < \frac{G}{K_e}\left(\frac{m}{e}\right)^2 A \Rightarrow \\ \Rightarrow Z_{net} \approx |Z_+ - Z_-| < 10^{-36}A \end{aligned} \tag{3.2.2}$$

This classical approximation sets an upper limit on the total number of like charges. It means that a neutron star has to be a neutral object and also that Z_+ or Z_- need not be zero. Since we have densities much larger than the normal nuclear matter density then we should expect that the nucleons could even be split into their ultimate components, the quarks. Several theoretical approximations are possible in guessing what's inside a neutron star and in this work we will study only the relativistic mean field theory approach with the baryon octet and the lightest leptons.

[1] Exceptionally in this calculation we use S.I. units.

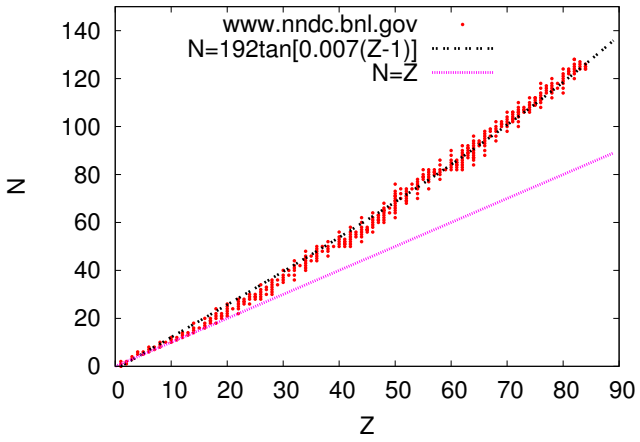

Figure 3.1: Neutron number (N) versus proton number (Z) and a fit to nuclei with half-lives greater than 3.8 months.

In figure 3.1 we can see that if A is small, nuclei with $N \approx Z$ are more stable than others. This changes as A gets larger, the more stable nuclei obey the equation $N \approx 192\tan[0.007(Z-1)]$ [21] so if we think of $Z = 82$ (Pb) we get $N \approx 122$ so a much greater number of neutrons than that of protons, though it is a very stable nucleus with a very long half-life of $\tau_{1/2} > 1.4 \times 10^{17}$ years. A neutron star can be highly isospin asymmetric, it is only required that the total electrical charge be zero. Strangeness was discovered during a cosmic ray study in 1947 in which a product of the collision between a proton and a nucleus was found to live for a longer time than was expected, 10^{-10} seconds, instead of the 10^{-23} seconds. The particle was named Λ-particle and the property that made it live for so long was coined "strangeness" and that name persisted and became the name of one of the quarks from which the Λ is built (see table 3.1). A shorter lifetime (10^{-23} seconds) was expected because it was a reaction in which the strong force was involved and that usually leads to very short lifetimes. This was later developed into a new conservation law called the "conservation of strangeness". If a particle has a strange quark, this is denoted by the quantum number S=-1. Strong or electromagnetic decays preserve strangeness. Λ has a mass of 1115.6 MeV and there is no lighter particle in which it can decay which has the strange quark so this quark is transformed into another quark in the decay, this can only happen by the weak interaction which leads to longer lifetimes. Strangeness is produced abundantly in nuclear reactions at high energies. Strangeness need not be conserved on a neutron star nor it is forcibly zero [10]. Nucleons in their fundamental state are devoid of strangeness and therefore nuclei in their fundamental state are also non-strange.

Baryon	Mass (MeV)	Charge	Quark content	Principal decays	Half-life
Proton	938.27	+1	uud	stable	$> 2.1 \times 10^{29}$ years
Neutron	939.57	0	udd	$p + e^- + \bar{\nu}_e$	881.5 ± 1.5 s
Λ	1115.6	0	uds	$p\pi^-$,$n\pi^0$	2.63×10^{-10} s
Σ^+	1189.4	+1	uus	$p\pi^0$,$n\pi^+$	0.8×10^{-10} s
Σ^0	1192.5	0	uds	$\Lambda\gamma$	6×10^{-20} s
Σ^-	1197.3	-1	dds	$n\pi^-$	1.48×10^{-10} s
Ξ^0	1314.9	0	uss	$\Lambda\pi^0$	2.90×10^{-10} s
Ξ^-	1321.3	-1	dss	$\Lambda\pi^-$	1.64×10^{-10} s

Table 3.1: Spin $\frac{1}{2}$ baryons and some of their properties.

Higher densities than the normal nuclear density such as those occurring in neutron stars will rise the Fermi energy and nucleons obey the Pauli principle so those protons and neutrons on the top Fermi levels are likely to transform into other heavier baryons, possibly strange ones. Table 3.1 lets us know all the spin $1/2$ baryons with or without strangeness, the baryon octet.

3.3 Chemical equilibrium in a star

Many reactions occur during the evolution of a neutron star until it reaches its final thermodynamic equilibrium (thermal equilibrium, mechanical equilibrium, radiative equilibrium, and chemical equilibrium) state (in this work, at zero temperature, which, on the nuclear scale is $T \approx 10^{10}$ K). Many different reactions may occur during its evolution to equilibrium, semileptonic reactions, hadron reactions, etc. Charge and baryon number are conserved on the lifetime of the star. Many reactions end up by creating leptons, photons and neutrinos. We expect that neutrinos and photons diffuse out of the star until no more reactions are possible, leaving the star in a degenerate state. In this state we assume that some of the reactions taking place inside the star are

$$B_1 \to B_2 + l + \bar{\nu}_l \tag{3.3.1a}$$

$$B_2 + l \to B_1 + \nu_l \tag{3.3.1b}$$

where B_i are baryons and l are the two lightest leptons. The data on nucleon-hyperon (NH) interactions and hyperon-hyperon (HH) are scarce and still have a lot of uncertainties contrary

to the complete and precise data on NN interactions. Above a certain energy, baryon-baryon interactions allow the possibility of the conversions

$$\Lambda + p \rightarrow \Sigma^{+} + n,\ \Lambda + p \rightarrow \Sigma^{0} + p \tag{3.3.2}$$

taking place. There are many other possibilities. Knowing how strong the connection of hyperons to neutrons and protons is very important to know how a neutron star may be populated by these particles. We can write for charge neutrality and chemical equilibrium

$$\sum_{i=1}^{8} \left(\rho_{B_i}^{(+)} + \rho_{l_i}^{(+)} \right) = \sum_{i=1}^{8} \left(\rho_{B_i}^{(-)} + \rho_{l_i}^{(-)} \right) \tag{3.3.3a}$$

$$\mu_i - b_i \mu_n = q_i \mu_l,\ \mu_S = 0 \tag{3.3.3b}$$

where ρ_{B_i} is the ith baryon density, ρ_{l_i} is the ith lepton density. The $(+)$ and $(-)$ superscripts indicate the positive or negative charges respectively. b_i is the baryonic number (0 or 1) and q_i the electric charge (-1 or 1). μ_n is the chemical potential of the neutron, μ_l is the chemical potential of the lepton l and μ_i is the chemical potential of the baryons or the leptons. μ_S is the strangeness chemical potential which is zero because on the any macroscopic timescale strangeness is not conserved.

Chapter 4

ASTROPHYSICS APPLICATION

4.1 Formalism

We now present the hadronic equation of state (EOS) used in this work. It is an extension of NLWM. In this model the nucleons are coupled to the neutral scalar σ, the iso-scalar-vector ω^μ and isovector-vector $\vec{\rho}_\mu$ mesons. We include simultaneously the σ-ρ and the ω-ρ meson dimensionless couplings Λ_σ and Λ_ω respectively. The Lagrangian density reads

$$\begin{aligned}\mathcal{L} = \sum_{j=1}^{8} \bar{\psi}_j \left[\gamma_\mu \left(i\partial^\mu - g_{\omega j}\omega^\mu - g_{\rho j}\vec{\tau}_j \cdot \vec{\rho}^{\,\mu}\right) - m_j^*\right] \psi_j \\ + \sum_{l=1}^{2} \bar{\psi}_l \left(i\gamma_\mu \partial^\mu - M_l\right) \psi_l \\ + \frac{1}{2}\partial_\mu\sigma\partial^\mu\sigma - \frac{1}{2}m_\sigma^2\sigma^2 - \frac{\kappa}{3!}\sigma^3 - \frac{\lambda}{4!}\sigma^4 \\ - \frac{1}{4}\Omega_{\mu\nu}\Omega^{\mu\nu} + \frac{1}{2}m_\omega^2\omega_\mu\omega^\mu + \frac{1}{4!}\xi g_\omega^4 \left(\omega_\mu\omega^\mu\right)^2 \\ - \frac{1}{4}\vec{R}_{\mu\nu}\vec{R}^{\mu\nu} + \frac{1}{2}m_\rho^2\vec{\rho}_\mu \cdot \vec{\rho}^{\,\mu} \\ + g_\rho^2\vec{\rho}_\mu \cdot \vec{\rho}^{\,\mu}\left[\Lambda_\sigma g_\sigma^2\sigma^2 + \Lambda_\omega g_\omega^2\omega_\mu\omega^\mu\right] \end{aligned} \tag{4.1.1}$$

where $m_j^* = m_j - g_{\sigma j}\sigma$ is the baryon effective mass, $\Omega_{\mu\nu} = \partial_\mu\omega_\nu - \partial_\nu\omega_\mu$, $\vec{R}_{\mu\nu} = \partial_\mu\vec{\rho}_\nu - \partial_\nu\vec{\rho}_\mu - g_\rho\left(\vec{\rho}_\mu \times \vec{\rho}_\nu\right)$, g_{ij} are the coupling constants of the mesons $i = \sigma, \omega, \rho$ with the baryon j, m_i is the mass of the meson i and l represents the leptons e^- and μ^-. The couplings κ ($\kappa = 2m_n g_\sigma^3 b$) and λ ($\lambda = 6g_\sigma^4 c$) are the weights of the non-linear scalar terms and $\vec{\tau}$ is the isospin operator. The sum over j in (4.1.1) extends over the octet of the lightest baryons $\{n, p, \Lambda, \Sigma^-, \Sigma^0, \Sigma^+, \Xi^-, \Xi^0\}$.

We established the values for the couplings Λ_σ and Λ_ω for symmetric nuclear matter and then we applied those values to the resulting EOS from (4.1.1). After that, we get the various profiles

for the resulting stars from TOV, maximum masses, maximum radii, particle populations dependence on either of the couplings. The mean field approximation to the equations of motion is:

$$\begin{aligned}
\sigma_0 &= \frac{g_\sigma}{m^2_{\sigma,eff}} \sum_B \frac{x_{\sigma B}}{\pi^2} \int_0^{k_F^B} \frac{m_B^* \, k^2 \, dk}{\sqrt{k^2 + {m_B^*}^2}} \\
\omega_0 &= \frac{g_\omega}{m^2_{\omega,eff}} \sum_B \frac{x_{\omega B} \left(k_F^B\right)^3}{3\pi^2}, \\
\rho_{03} &= \frac{g_\rho}{m^2_{\rho,eff}} \sum_B \frac{x_{\rho B} \tau_{3B} \left(k_F^B\right)^3}{3\pi^2}
\end{aligned}$$

where the meson effective masses are defined as:

$$\begin{aligned}
m^2_{\sigma,eff} &= m^2_\sigma + \frac{k}{2}\sigma_0 + \frac{\lambda}{6}\sigma_0^2 - 2\Lambda_\sigma g^2_\sigma g^2_\rho \rho^2_{03} \\
m^2_{\omega,eff} &= m^2_\omega + \frac{\xi}{6} g^4_\omega \omega_0^2 + 2\Lambda_\omega g^2_\omega g^2_\rho \rho^2_{03}, \\
m^2_{\rho,eff} &= m^2_\rho + 2g^2_\rho \left[\Lambda_\omega g^2_\omega \omega_0^2 + \Lambda_\sigma g^2_\sigma \sigma_0^2\right]
\end{aligned}$$

The EOS is changed by both mixing factors on the Lagrangian density 4.1.1 as we can see next in equations 4.1.4 and 4.1.5.

$$\begin{aligned}
\varepsilon = \frac{1}{2}m^2_\sigma\sigma^2 + \frac{\kappa}{3!}\sigma^3 + \frac{\lambda}{4!}\sigma^4 + \frac{1}{2}m^2_\omega\omega^2 + \frac{\xi}{8}(g_\omega\omega)^4 + \frac{1}{2}m^2_\rho\rho^2_{03} + \\
+3(g_\rho\rho_{03})^2\left[\Lambda_\omega(g_\omega\omega)^2 + \frac{\Lambda_\sigma}{3}(g_\sigma\sigma)^2\right] + \frac{1}{\pi^2}\sum_{i=1}^{8}\int_0^{k_i} k^2\sqrt{k^2 + (m_i - g_\sigma\sigma)^2}\, dk \\
+\frac{1}{\pi^2}\sum_{l=1}^{2}\int_0^{k_F^l} k^2\sqrt{m_l^2 + k^2}\, dk
\end{aligned} \tag{4.1.4}$$

$$\begin{aligned}
p = -\frac{1}{2}m^2_\sigma\sigma^2 - \frac{\kappa}{3!}\sigma^3 - \frac{\lambda}{4!}\sigma^4 + \frac{1}{2}m^2_\omega\omega^2 + \frac{\xi}{4!}(g_\omega\omega)^4 + \frac{1}{2}m^2_\rho\rho^2_{03} + \\
+(g_\rho\rho_{03})^2\left[\Lambda_\omega(g_\omega\omega)^2 + \Lambda_\sigma(g_\sigma\sigma)^2\right] + \frac{1}{3\pi^2}\sum_{i=1}^{8}\int_0^{k_i}\frac{k^4}{\sqrt{k^2 + (m_i - g_\sigma\sigma)^2}}\, dk \\
+\frac{1}{3\pi^2}\sum_{l=1}^{2}\int_0^{k_F^l} k^2\sqrt{m_l^2 + k^2}\, dk
\end{aligned} \tag{4.1.5}$$

The formula in which we are really interested in and that changes what happens to the EOS and ultimately, to neutron stars, is the symmetry energy, we can compare it to the symmetry energy on the NLWM model (2.2.28)

$$a_{sym} = \frac{k_F^2}{6\sqrt{k_F^2 + (m - g_\sigma\sigma)^2}} + \frac{g^2_\rho}{8}\frac{\rho}{m^2_\rho + 2g^2_\rho\left[\Lambda_\omega(g_\omega\omega)^2 + \Lambda_\sigma(g_\sigma\sigma)^2\right]} \tag{4.1.6}$$

and by this we can see that variations on the symmetry energy by the constants Λ_σ and Λ_ω cause significant changes in how a_{sym} grows with density. For neutron star matter consisting of a neutral mixture of baryons and leptons, the β equilibrium condition without neutrino trapping are given by

$$\begin{aligned} \mu_p &= \mu_{\Sigma^+} = \mu_n - \mu_e \\ \mu_\Lambda &= \mu_{\Sigma^0} = \mu_{\Xi^0} = \mu_n \\ \mu_{\Sigma^-} &= \mu_{\Xi^-} = \mu_n + \mu_e \\ \mu_\mu &= \mu_e \end{aligned} \tag{4.1.7}$$

where μ_i is the chemical potential of species i. The chemical potentials of baryons and leptons are given by

$$\begin{aligned} \mu_B &= \sqrt{k_F^{B\,2} + m_B^{*\,2}} + g_{\omega B}\omega_0 + g_{\rho B}\tau_{3B}\rho_{03} \\ \mu_l &= \sqrt{k_F^{l\ 2} + m_l^2}. \end{aligned} \tag{4.1.8}$$

and the charge neutrality condition is written by

$$\rho_p + \rho_{\Sigma^+} = \rho_e + \rho_\mu + \rho_{\Sigma^-} + \rho_{\Xi^-}, \tag{4.1.9}$$

where $\rho_i = \left(k_F^i\right)^3 / \left(3\pi^2\right)$ is the number density of species i. In this work, we employ the NL3 parameter set of the NLWM listed in table 4.1 which has the saturation properties listed in table 4.2. The meson-hyperon and the strange meson-hyperon coupling constants $g_{\omega H}$, $g_{\rho H}$ and $g_{\sigma H}$ are determined by using SU(6) symmetry

$$\frac{1}{3}g_{\omega N} = \frac{1}{2}g_{\omega\Lambda} = \frac{1}{2}g_{\omega\Sigma} = g_{\omega\Xi}, \tag{4.1.10a}$$

$$g_{\rho N} = g_{\rho\Lambda} = \frac{1}{2}g_{\rho\Sigma} = g_{\rho\Xi} \tag{4.1.10b}$$

$$2g_{\sigma\Lambda} = 2g_{\sigma\Sigma} = g_{\sigma\Xi} = -\frac{2\sqrt{2}}{3}g_{\omega N} \tag{4.1.10c}$$

where N means nucleon ($g_{iN} \equiv g_i$). The scalar coupling constants are chosen to give reasonable potentials. The coupling constants $g_{\sigma H}$ of the hyperons with the scalar meson σ are adjusted to the potential depths $U_H^{(N)}$ felt by a hyperon H in symmetric nuclear matter at saturation following the relation

$$U_H^N = x_{\omega H}V_\omega - x_{\sigma H}V_\sigma \tag{4.1.11}$$

with $x_{i,H} = g_{i,H}/g_i$, $V_\omega \equiv g_\omega\omega_0$ and $V_\sigma \equiv g_\sigma\sigma_0$ are the nuclear potentials for symmetric nuclear matter at saturation density. For the present work we will fix $U_\Lambda^N = -28$ MeV, and use $U_\Sigma^N = -30,\ 0,\ 30$ MeV, and for U_Ξ^N we will use different values -18, and 0 MeV. All hyperon coupling ratios $\{g_{\sigma H}, g_{\omega H}, g_{\rho H}\}_{H=\Lambda,\Sigma,\Xi}$ are determined once the coupling constants $\{g_\sigma, g_\omega, g_\rho\}$ of the nucleon sector are given. The hyperons masses are taken to be $m_\Lambda = 1116$ MeV, $m_{\Sigma^+} = 1189$ MeV, $m_{\Sigma^0} = 1193$ MeV, $m_{\Sigma^-} = 1197$ MeV and $m_{\Xi^0} = 1315$ MeV, $m_{\Xi^-} = 1321$ MeV.

4.2 Results

The main objective of the work is to change the symmetry energy density dependence and look at what happens to the structure of a neutron star and how its radius and mass changes. We change the dependence of the symmetry energy on the density by changing its slope, L, at saturation density. We only use the original NL3 parameter set of Lalazissis, König, and Ring [6] to calculate all EOS for star calculations.

m_σ (MeV)	m_ω (MeV)	m_ρ (MeV)	g_σ	g_ω	g_ρ	b	c	ξ
508.194	783	763	10.217	12.868	8.948	0.002052	-0.002651	0

Table 4.1: **NL3** [6] parameter set. The nucleon mass is $m = 939$ MeV.

ρ_0 (fm^{-3})	$\mathcal{K}$ (MeV)	m^*/m	-B/A (MeV)	a_{sym} (MeV)	L (MeV)
0.148	271.76	0.60	16.299	37.2	118

Table 4.2: NL3 saturation properties.

The NL3 set has $\xi = \Lambda_\sigma = \Lambda_\omega = 0$ and provides a good fit to the ground-state properties of many nuclei. In this model symmetric nuclear matter saturates at $k_F = 1.30$ fm^{-1} with a binding energy per nucleon of $B/A = -16.25$ MeV and an incompressibility of $\mathcal{K} = 271$ MeV. The original NL3 parameter set predicts a symmetry energy of 37.4 MeV at saturation density and close to 25.68 MeV at $k_F = 1.15$ fm^{-1} [6]. In this work adjustments (see section 4.2.1) were made to fit the symmetry energy with a value of $a_{sym} = 25.68$ MeV at a Fermi momentum of $k_F = 1.15$ fm^{-1} for all parameter sets generated. We use this because we can find a common ground with known results for the Λ_ω coupling in the work of Horowitz [22] and is a way of checking that our results are correct.

4.2.1 Symmetric nuclear matter couplings

Using formula (4.1.6) we can get g_ρ as a function either of Λ_σ or Λ_ω

$$g_\rho^2 = \frac{m_\rho^2}{\frac{\rho}{8A_{sym}} - 2\left[\Lambda_\omega(g_\omega\omega)^2 + \Lambda_\sigma(g_\sigma\sigma)^2\right]} \tag{4.2.1}$$

where $A_{sym} = a_{sym} - \frac{k_F^2}{\sqrt{k_F^2+(m-g_\sigma\sigma)^2}}$. We can now select $\Lambda_\sigma = 0$ or $\Lambda_\omega = 0$ alternatively and get the coupling constants. We selected values of $k_F = 1.15$ fm^{-1} and $a_{sym} = 25.68$ MeV so as to be able to reproduce the same restrictions as Horowitz [22] did in Λ_ω and g_ρ. We also proceed the same way with the pairs (Λ_σ, g_ρ). The MFA equations of motion for ω and for σ are not disturbed by the Λ_σ or Λ_ω parameters because we are studying the values at $Y_p = 0.5$ (symmetric nuclear matter, $\rho_p = \rho_n$) and in this case we have $\rho_{03} = 0$. Whenever the denominator in (4.2.1) is zero g_ρ diverges. We can check algebraically where the divergence happens by solving the equation

$$\frac{\rho}{8A_{sym}} - 2\left[\Lambda_\omega(g_\omega\omega)^2 + \Lambda_\sigma(g_\sigma\sigma)^2\right] = 0 \tag{4.2.2}$$

alternatively picking $\Lambda_\omega = 0$ and $\Lambda_\sigma = 0$ we get the system of equations that defines the Λ_i where g_ρ diverges:

$$\Lambda_\omega = \frac{\rho}{16 A_{sym} (g_\omega \omega)^2} \tag{4.2.3a}$$

$$\Lambda_\sigma = \frac{\rho}{16 A_{sym} (g_\sigma \sigma)^2} \tag{4.2.3b}$$

Divergence happens when $\Lambda_\sigma = 0.04925$ and $\Lambda_\omega = 0.08019$, this can be seen in figure 4.1. We should note that g_ρ varies with Λ_σ in almost the same way as with Λ_ω, the difference is that it diverges sooner with Λ_σ than with Λ_ω. This will force us to choose the values of L carefully so as

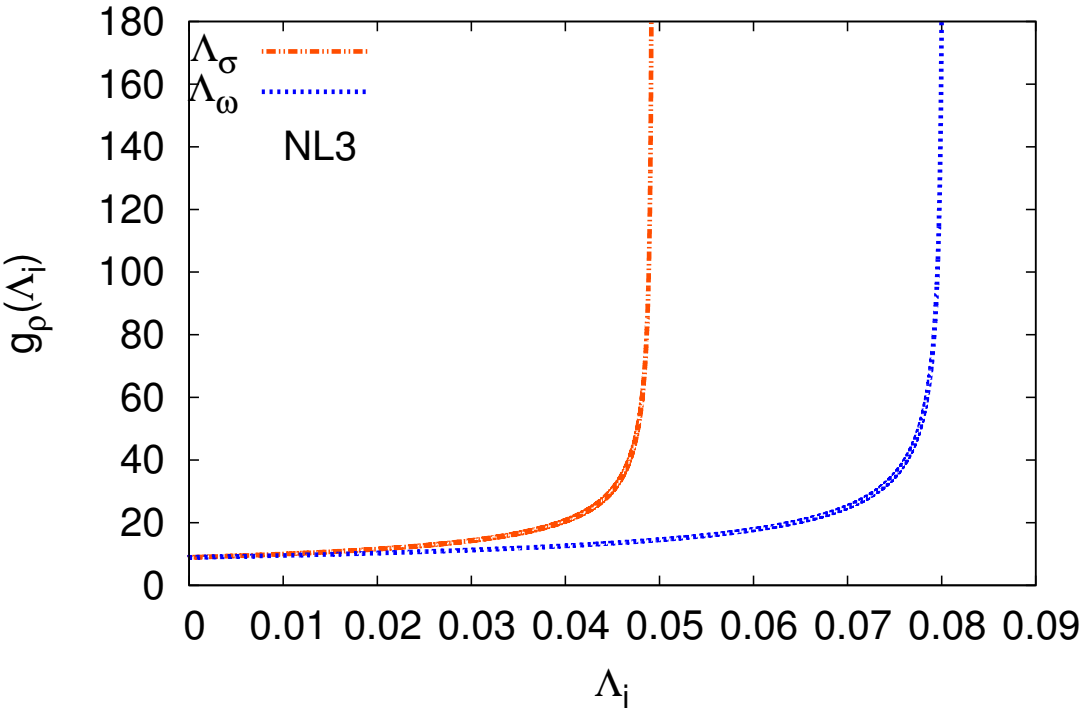

Figure 4.1: g_ρ versus Λ_i in correspondence with σ-ρ mixing and the ω-ρ mixing in symmetric nuclear matter. We can clearly distinguish a greater restriction on Λ_σ values than the restriction for Λ_ω.

to not introduce numerical errors or, more importantly, non-physical solutions. We will see how this works in subsection 4.2.2. Figure 4.2 gives L at saturation density as a function of either Λ_ω or Λ_σ. We can see here the smaller range of values for Λ_σ than for the Λ_ω coupling. This is in agreement with what happens with g_ρ in figure 4.1. We then chose specific values of the slope L to fix pairs of both coupling constants (Λ_ω, g_ρ) and (Λ_σ, g_ρ) using both $L(\rho_0, \Lambda_i)$ curves. We can visualize this by drawing an imaginary horizontal line in figure 4.2 for, for example $L = 50$ MeV. Then we will have two intersections, one for $L(\rho_0, \Lambda_\omega) = 50$ MeV and one for $L(\rho_0, \Lambda_\sigma) = 50$ MeV.

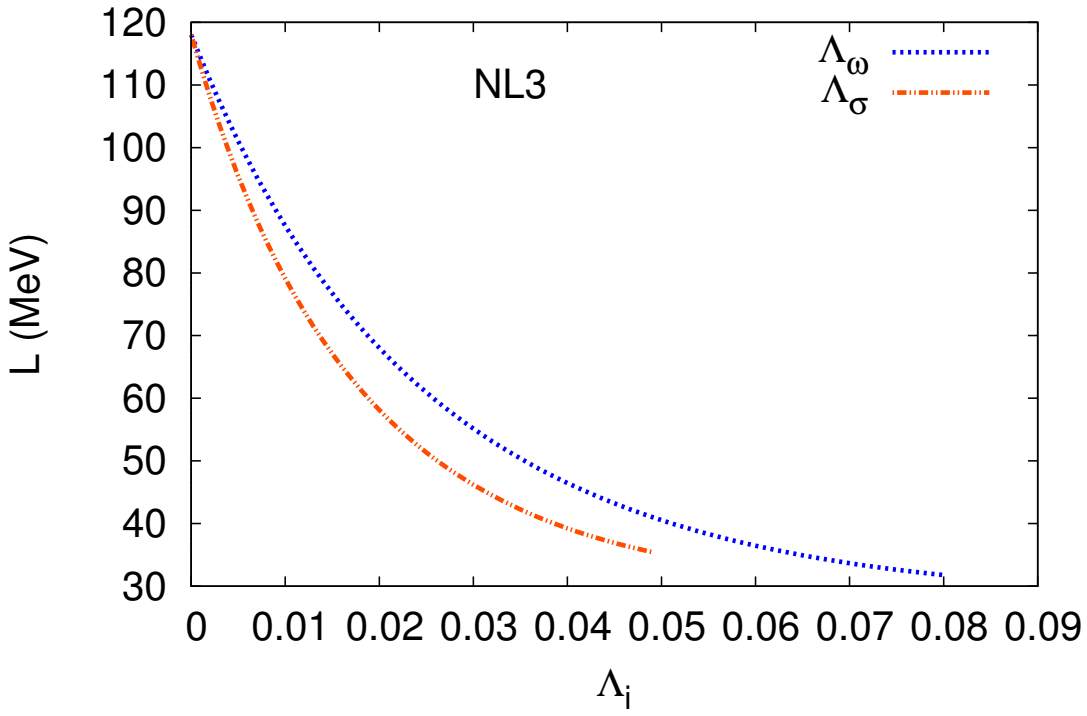

Figure 4.2: Slope of the symmetry energy at saturation density versus the Λ_σ and Λ_ω couplings.

This will let us choose, uniquely, values for Λ_σ and Λ_ω. Then, using Λ_σ in $g_\rho(\Lambda_\sigma)$ will fix the pair (Λ_σ, g_ρ). In the same manner, using Λ_ω in $g_\rho(\Lambda_\omega)$ will fix the pair (Λ_ω, g_ρ). This way we can fix the couplings for any value of L. We can see in figure 4.2 that the influence of Λ_σ systematically lowers the value of L more than the effect of Λ_ω as each Λ_i grows. As we can see in figure 4.3 the range of values of a_{sym} is $[29.32, 37.2]$ MeV and the range for L is $[41, 118]$ MeV. Many fits of the coupling constants of relativistic mean field (RMF) theory to nuclear matter have an interval of symmetry energy at saturation density of $a_{sym} \in [31, 38]$ at best [8]. Phenomenological values of the slope of the symmetry energy lie in the range $L \in [30, 80]$ [18]. Other authors have extrapolated other ranges. This work obtains a different range of values for L. We will see next how we get consistent values for the EOS to use in TOV (3.1.1) if we work in the range $L \in [41, 118]$ in the next section. The slope L of the symmetry energy tells us how fast a_{sym} will grow with the increase of density. Lower L means a less accentuated growth, we can see this in figure 4.4 where three values of L are plotted, the original 118 MeV of the NL3 parameter set two for each $L = 80$ MeV and $L = 50$ MeV for Λ_σ and Λ_ω. The influence of the mixture ω-ρ lowers the growth of a_{sym} more than the σ-ρ mixture. If L is lower then a_{sym} gets lower for all densities. We should recall that the greater the difference $\rho_n - \rho_p$ is, the greater is the reducing of the binding energy per nucleon.

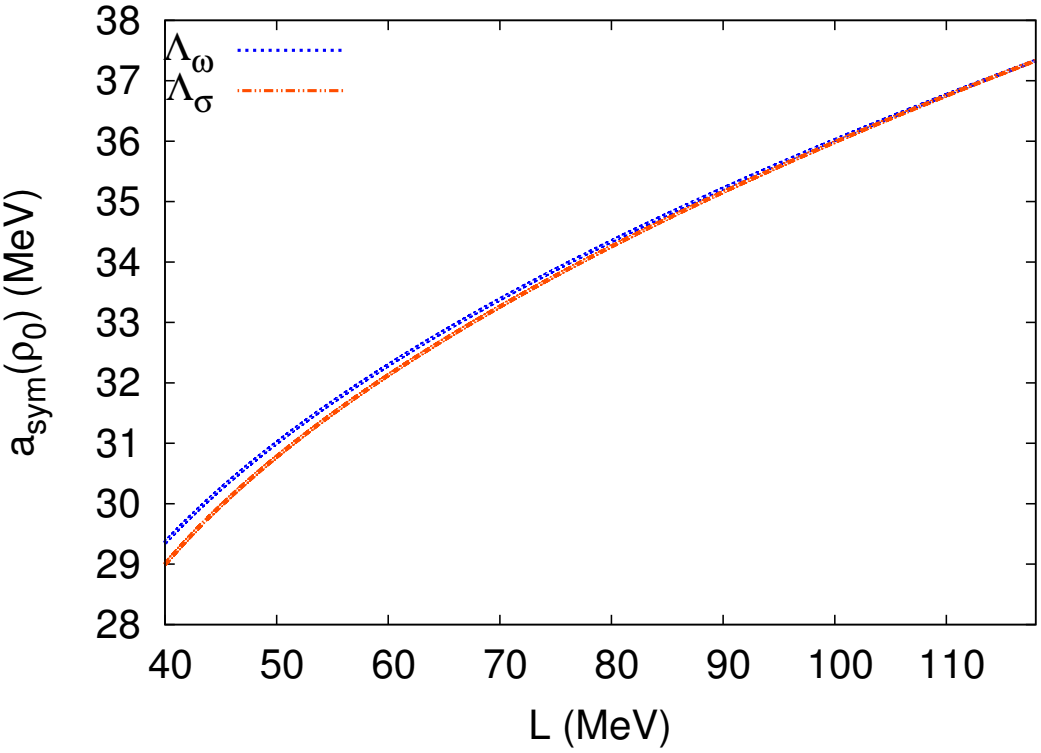

Figure 4.3: Symmetry energy at saturation density versus L. We can see here what are both ranges for L and for a_{sym} at saturation density simultaneously.

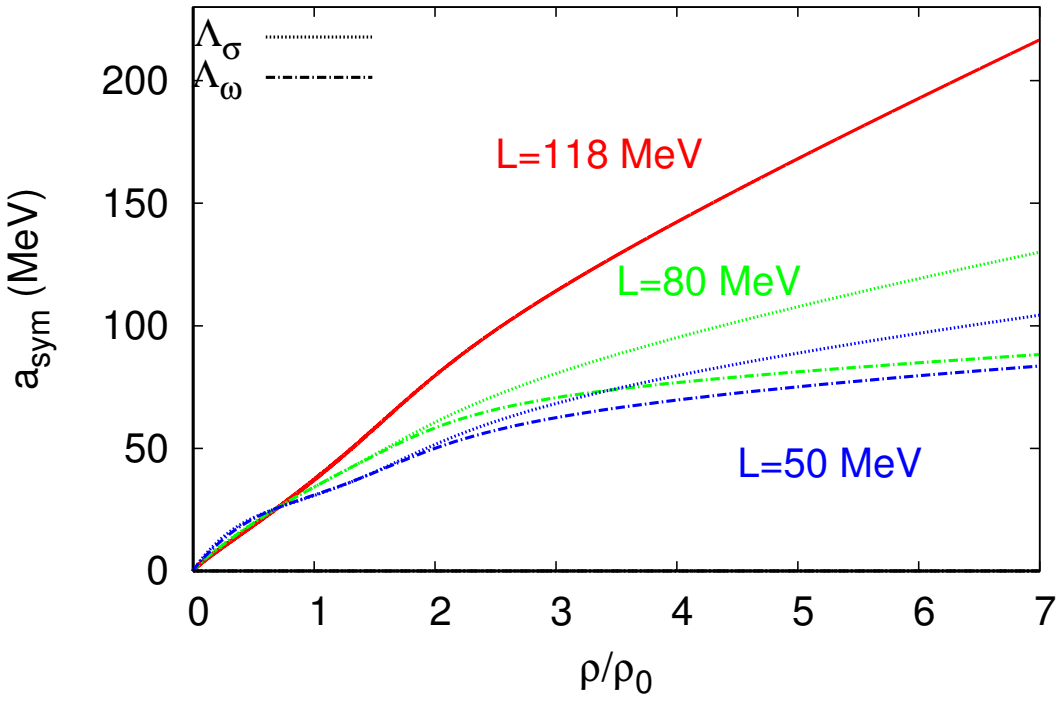

Figure 4.4: Symmetry energy versus density with different L values and the corresponding coupling constants Λ_ω (dot-dashed line) and Λ_σ (dotted line). The original NL3 set is the full line in red ($L = 118$ MeV). The green lines are for $L = 80$ MeV and the blue lines for $L = 50$ MeV.

4.2.2 Nuclear matter in β equilibrium

As we saw in section 3.1 the TOV equation is solved using a certain set of values of the energy density and the pressure (which we can, without loss of meaning, call EOS) and by setting the boundary conditions (3.1.2) which require that at radius R (the radius of the star) the pressure has to be zero. This way the binding energy of our model must not have inflection points in which the pressure is zero before the density reaches zero. In figure 4.5 we show the maximum

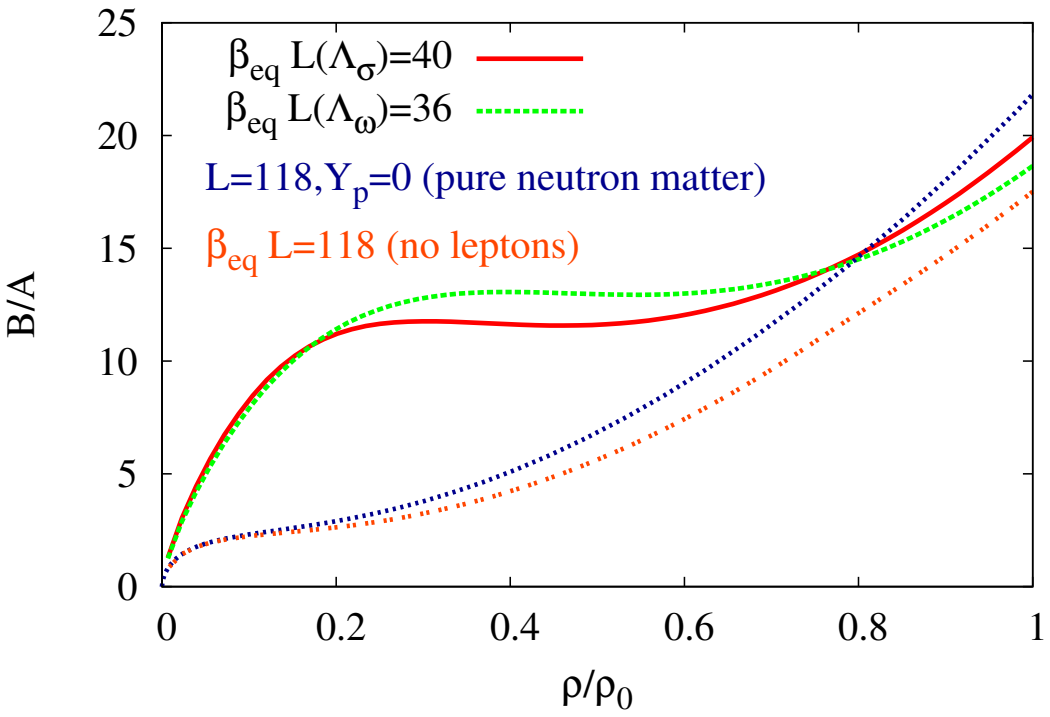

Figure 4.5: Binding energy per nucleon versus density for different values of L for nuclear matter in β equilibrium and in pure neutron matter.

values of L for the different mixtures σ-ρ and ω-ρ for which there still exist inflection points in the binding energy i.e., ranges of density for which the pressure still changes signal from negative to positive. This inflection point is correlated with the fact that the symmetry energy for symmetric matter is being forced to go through the point $k_F = 1.15$ fm^{-1} ($\rho = 0.69\rho_0$) with $a_{sym} = 25.68$ MeV. This can be easily seen if we compare figure 4.4 with figure 4.5. Further analysis shows that the minimum value of L that we can trust to generate a star that obeys $p(r = R) = 0$ at $\rho = 0$ for each of the parameters is $L = 36.5$ MeV for the ω-ρ mixing and $L = 41$ MeV for σ-ρ mixing. We can verify in figure 4.6 that the pressure is always positive for the values of L presented in any of the mixtures σ-ρ or ω-ρ. We can also see in figure 4.6 that pressure rises very fast with density and, for low densities (up to $0.6\rho_0$) the pressure oscillates slightly for low L in correlation with the symmetry energy being forced to go through $\rho = 0.69\rho_0$ and $a_{sym} = 25.68$ MeV. The

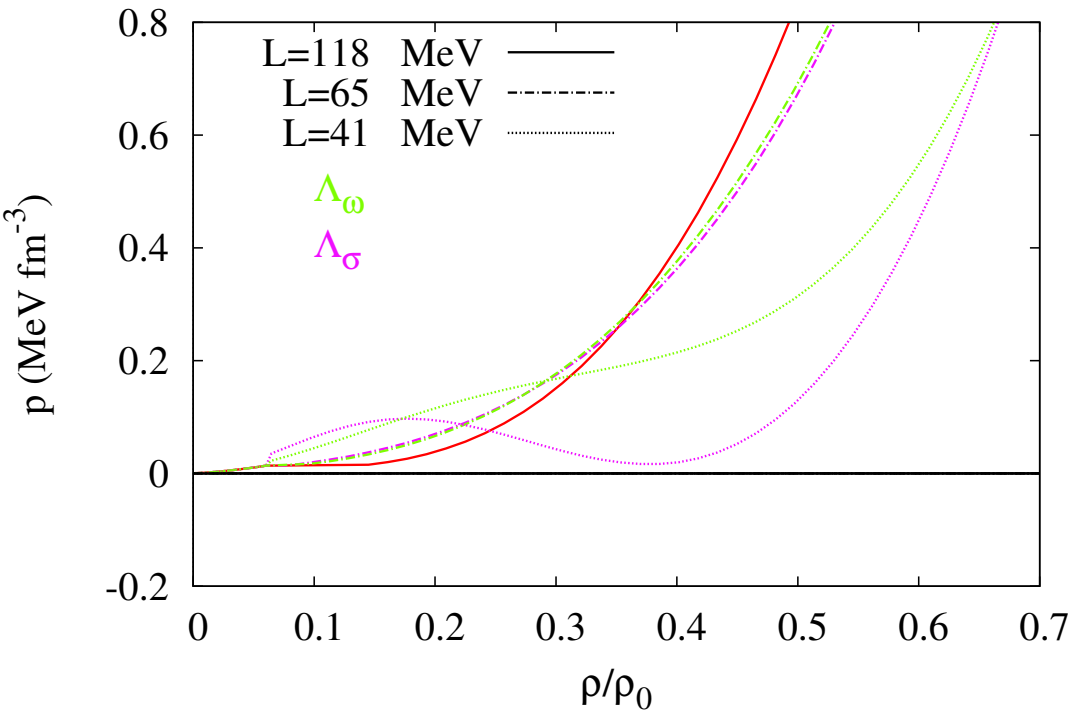

Figure 4.6: Pressure versus density for different values of L for nuclear matter in generalised β equilibrium. In pink is the σ-ρ mixing and in green is the ω-ρ mixing.

behaviour of the pressure is directly correlated also with the binding energy per nucleon because the pressure is defined as the derivative of the binding energy per nucleon times ρ^2 (see formula (2.2.13)). The L value was carefully selected so as to the pressure never reach zero before $\rho = 0$ for us to get a star with zero density at the surface. For low densities, which means up to $\rho/\rho_0 \sim 0.06$ we have included the BPS [23] equation of state values in the figure and in all inputs to solving the TOV. However, although for $L = 41$ MeV ω-ρ and σ-ρ mixings have $p > 0$, there is a region of instability with $\frac{\partial p}{\partial \rho} < 0$ in the σ-ρ mixing. No homogeneous matter occurs in this range of densities for the σ-ρ mixing at $L = 41$ MeV. We see in figure 4.7 that all the particle fractions change with density. Charge neutrality is achieved firstly, for low densities, by having the same number of protons and electrons but, as density rises the proton number becomes greater than the number of electrons but this charge imbalance is compensated by the appearance of muons. The rising of the numbers of charged particles at high densities lowers the number of neutrons in the mixture. Having either of the mixings, lower values of L will decrease the fraction of charged particles and increase the fraction of neutrons simultaneously in comparison with the original NL3 parameter set. In figure 4.7 we only show the σ-ρ mixing which behaves in a very similar manner as the ω-ρ mixing: it will, as L decreases, for densities larger than the saturation density, lower the fraction of charged particles and increase the fraction of neutrons. The direct

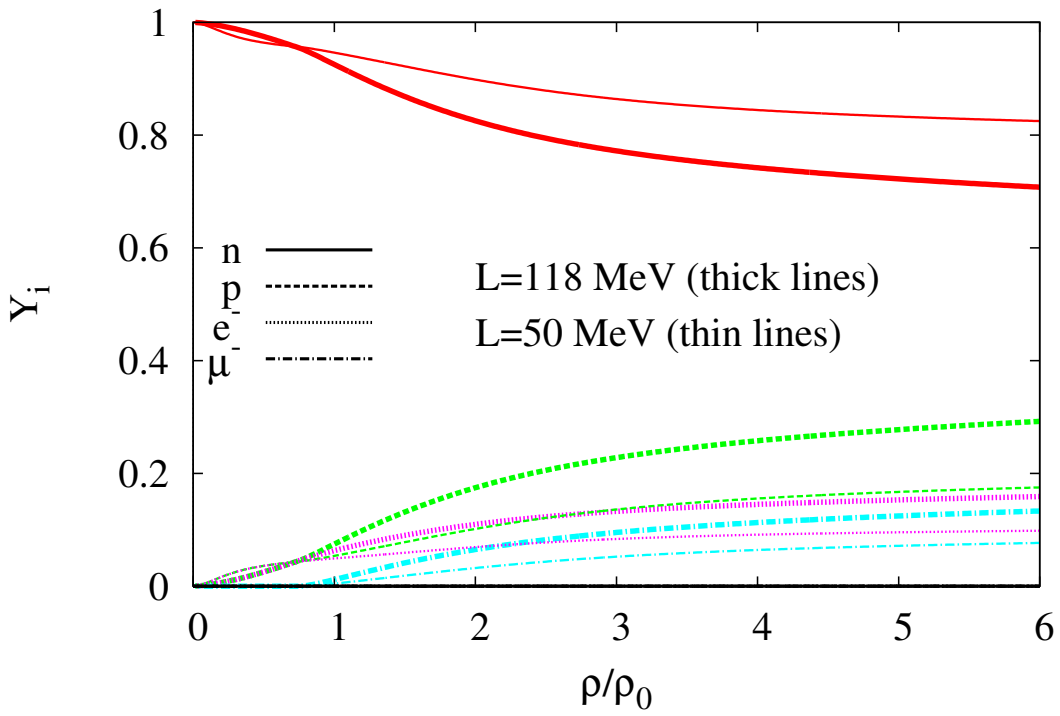

Figure 4.7: Fraction ($Y_i = \rho_i/\rho$) of neutrons, protons, electrons and muons in β equilibrium as a function of density for two values of the slope of the symmetry energy.

Urca process for nucleons refers both to neutron β decay

$$n \to p + e^- + \bar{\nu}_e \tag{4.2.4}$$

and electron capture on protons

$$p + e^- \to n + \nu_e \tag{4.2.5}$$

and contributes highly to the rapid cooling of neutron stars [24] because of the neutrino emissions. Neutrino and anti-neutrino Fermi momentum is much less than any of the momenta from the other particles [25] and we can neglect it. For the direct Urca process to occur we must admit $k_{F_p} + k_{F_e} \geq k_{F_n}$. When stellar matter consists only of protons, neutrons and electrons charge neutrality forces us to impose $\rho_e = \rho_p$. In this manner we get that, for the direct Urca process to occur, $\rho_p \geq \rho/9$. In the case we are studying now the muon has a role in this process because it shares a part in the charge neutrality condition ($\rho_p = \rho_e + \rho_\mu$) so we must meet this problem in a different manner. Lattimer, Pethick and Prakash [25, 26] establish that the direct Urca process particle fraction $x_{\rm DU}$ is defined by

$$x_{\rm DU} = \frac{1}{1 + (1 + x_e^{1/3})^3} \tag{4.2.6}$$

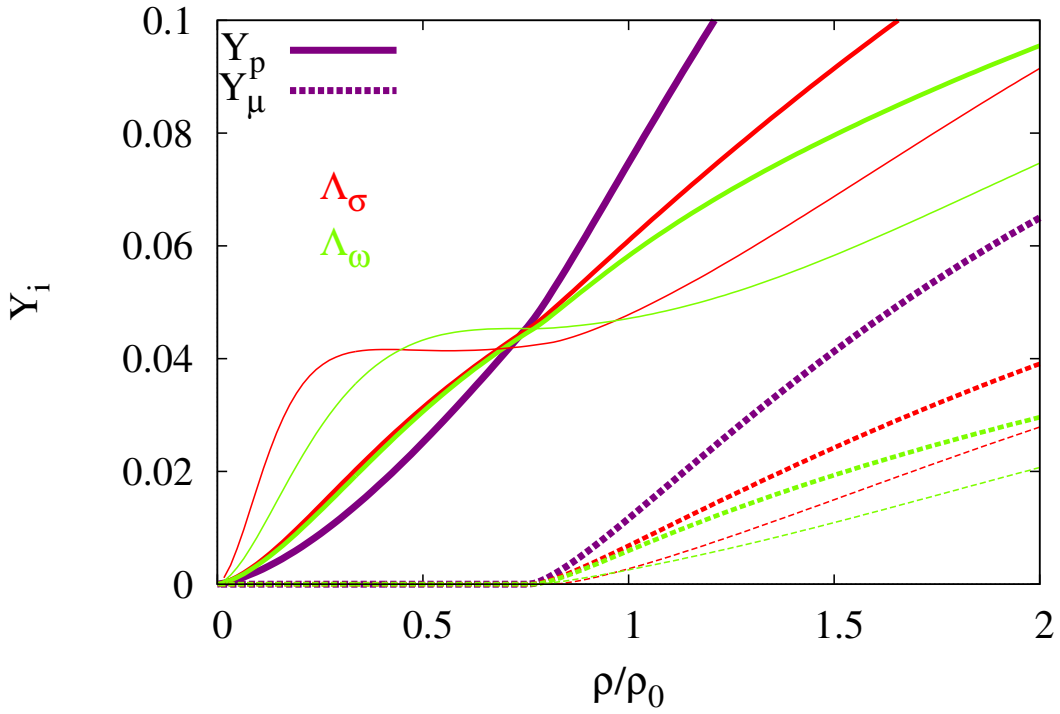

Figure 4.8: Zoom of particle fraction versus density, in this case for protons (full lines) and muons (dashed lines). $L = 118$ MeV (thick lines, purple), $L = 65$ MeV (medium lines), $L = 41$ MeV (thin lines). The Λ_σ (red lines) and Λ_ω (green lines) couplings are also present.

where $x_e = \frac{\rho_e}{\rho_e + \rho_\mu}$. This number ($x_e$) is 1 for the case where there are no muons in the mixture and in this case we reproduce exactly the case we already mentioned $\rho_p > \rho/9$ to have the direct Urca process. To establish an upper limit to the process we can assume that $\rho_e \approx \rho_\mu$ and get $x_e = 1/2$ which turns $x_{\rm DU}$ into 0.148. So for each different model EOS we will get different values for the onset of the direct Urca process within the range defined by the lower limit $U_{\rm inf} = 1/9$ and the upper limit $U_{\rm sup} = 0.148$.

Leptons	Mass (MeV)	Charge	Principal decays	Half-life
Electron e^-	0.511003	-1	stable	∞
Muon μ^-	105.659	-1	$e^- + \bar{\nu}_e + \nu_\mu$	2.197×10^{-6} s

Table 4.3: Leptons used in this work and some of their properties.

The masses and charges of the leptons and other properties that we used in this work are in table 4.3. As can be seen from figure 4.9 the decrease in L makes the fraction of all the charged

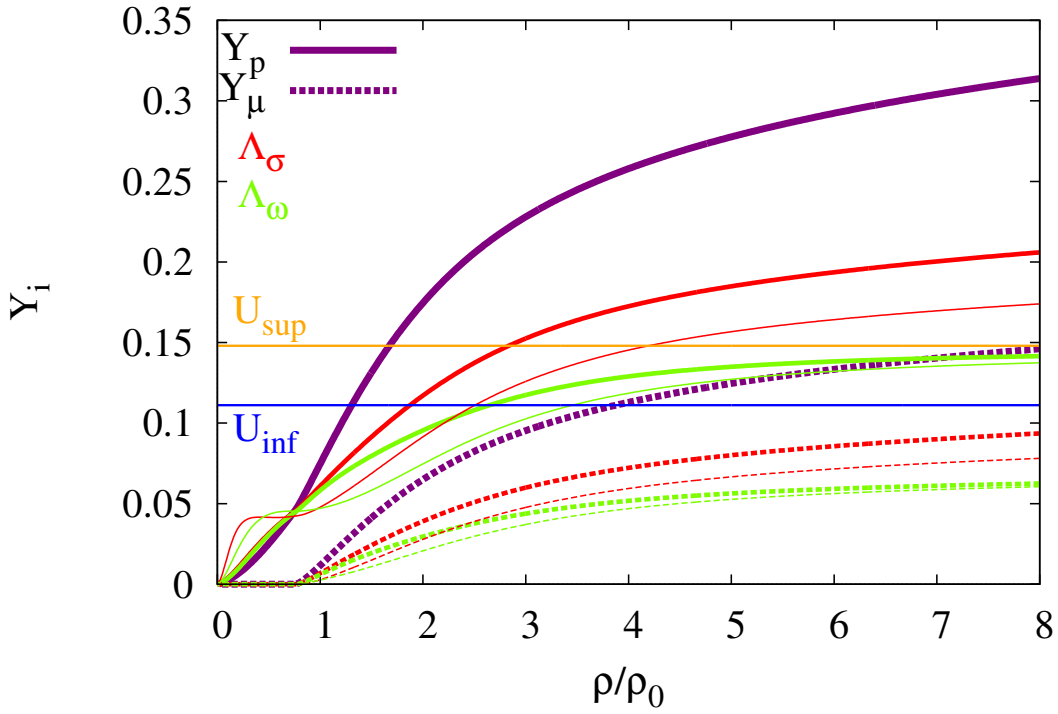

Figure 4.9: Proton (full line) and muon (dashed line) fractions versus density variation with L =(118 MeV thick lines (NL3 original) ,65 MeV medium lines,41 MeV thin lines) for the Λ_σ (red) and Λ_ω (green) couplings. Also drawn are the upper $x_{\rm DU} = 0.148 = U_{\rm sup}$ and lower $x_{\rm DU} = 1/9 = U_{\rm inf}$ limits of the Urca process.

particles increase slower and also saturate at a lower value than with higher L. The Urca process is reached at higher densities with decreasing L. We can see this in the plot of figure 4.10. The effect of Λ_ω on the onset of the Urca process is stronger than the effect of Λ_σ i.e., with Λ_ω it appears at higher densities than with Λ_σ, we can see that on figure 4.10. Also, the range of densities is from $1.3\rho_0$ to $3.4\rho_0$ as L varies from 41 MeV to 118 MeV. Figure 4.8 allows us to verify that the way the proton fraction increases is correlated with how the symmetry energy grows at densities lower than the saturation density (compare figure 4.4). When $L \approx 41$ MeV there is a very fast increase of the symmetry at low densities and also on the proton and electron fractions. The symmetry energy is being forced to go through 25.67 MeV at $k_F = 1.15$ fm^{-1} with a low L then it has to "compensate" by giving rise to a great binding at low densities and this is achieved by a great increase in the number protons/electrons.

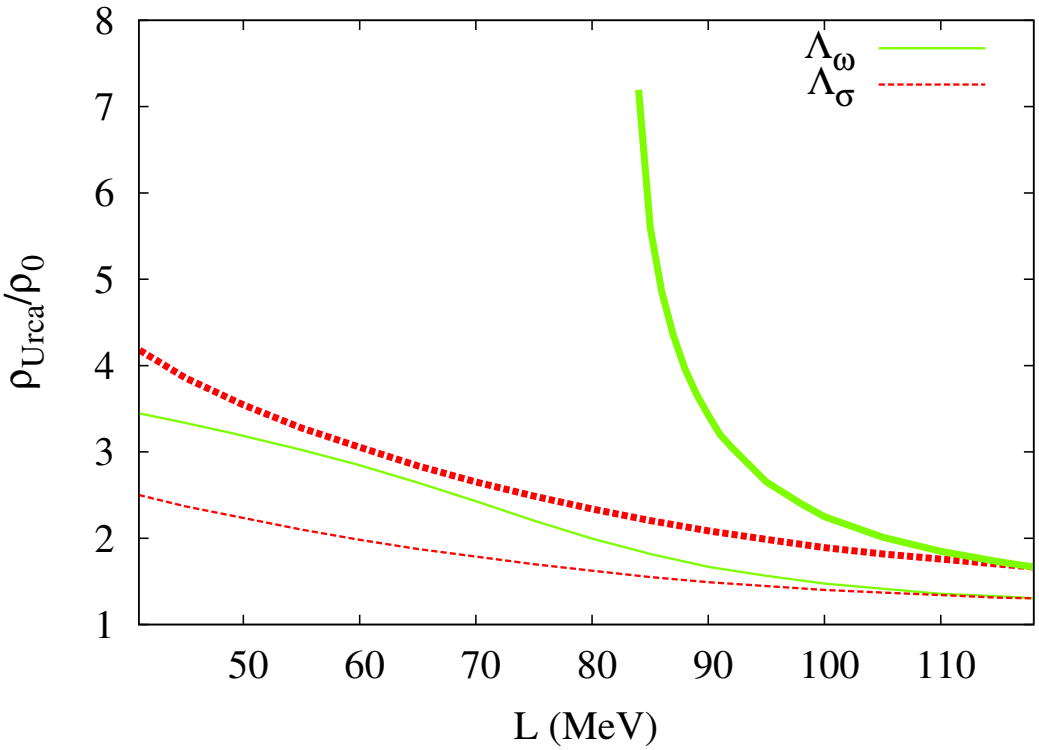

Figure 4.10: Onset of the direct Urca process versus L. The lower limit $U_{\text{inf}} = 1/9$ are the thin lines and the upper limit $U_{\text{sup}} = 0.148$ are the thick lines. Both couplings are shown, Λ_σ (dashed lines) and Λ_ω (full lines).

4.2.3 L influence on star variables

Solving the TOV equation is the main purpose of this work once we have the EOS modified with the nonlinear ω-ρ and σ-ρ terms. In first approximation we make the EOS have protons, neutrons, electrons and muons in chemical equilibrium and charge neutral. As we saw before, changing L changes the density dependence of the symmetry energy an here we show the resulting effect of $a_{sym}(\rho, L)$ on the maximum gravitational and baryonic mass and radius of a neutron star and other variables. We show also what happens to the central energy density and the central density. Though we made calculations both of the EOS and the TOV for a great number of L values (from 40 to 118 MeV) we here present only some of them, just enough to see the main trend of the results. Tables 4.4 and 4.5 list the values obtained as function of L of the maximum gravitational mass M_{max}, the maximum baryonic mass M_{Bmax}, the central energy density ε_0 and the total central density ρ_c. What we see in table 4.4 is a systematic decrease in maximum gravitational mass down to $L = 60$ MeV and then a slight increase until $L = 40$ MeV. The same thing happens to the maximum baryonic mass. The radius systematically decreases with decreasing L. The central energy density and total density increase with decreasing L. The TOV system of equations (3.1.1) generates a family of neutron stars, one for each EOS [1]. Changing L has made significant changes to our EOS [(4.1.4) and (4.1.5)]. It has generated two EOS for each

L	$M_{max}(M_\odot)$	$M_{Bmax}(M_\odot)$	R (km)	ε_0(fm^{-3})	ρ_c(fm^{-3})
118.0	2.793	3.331	14.068	4.074	0.621
110.0	2.787	3.325	14.020	4.093	0.624
100.0	2.781	3.320	13.948	4.135	0.630
90.00	2.776	3.318	13.893	4.150	0.632
80.00	2.773	3.317	13.843	4.172	0.636
70.00	2.771	3.319	13.796	4.192	0.639
60.00	2.770	3.322	13.758	4.195	0.640
50.00	2.771	3.327	13.711	4.197	0.641
41.00	2.772	3.334	13.651	4.208	0.643

Table 4.4: Variations of the maximum values of star variables (maximum mass M_{max}, maximum baryonic mass M_{Bmax}, radius R, central energy density ε_0 and central density ρ_c) with changing L, in this case for the σ-ρ mixing.

L	$M_{max}(M_\odot)$	$M_{Bmax}(M_\odot)$	R (km)	ε_0 (fm^{-3})	ρ_c (fm^{-3})
118.0	2.793	3.331	14.068	4.074	0.621
110.0	2.763	3.293	13.953	4.139	0.632
100.0	2.750	3.280	13.829	4.206	0.641
90.00	2.747	3.281	13.751	4.244	0.646
80.00	2.747	3.287	13.700	4.268	0.64965
70.00	2.750	3.296	13.661	4.267	0.64993
60.00	2.754	3.306	13.633	4.262	0.64990
50.00	2.759	3.317	13.612	4.258	0.64981
40.00	2.765	3.330	13.582	4.240	0.64824

Table 4.5: Variations of the maximum values of star variables (maximum mass M_{max}, maximum baryonic mass M_{Bmax}, radius R, central energy density ε_0 and central density ρ_c) with changing L, in this case for the ω-ρ mixing.

L, one for Λ_σ and one for Λ_ω. The results for the family of stars created for each L are plotted in figure 4.11 In both sets of (maximum) stars the Urca process definitely appears since for each of the sets the central minimum densities of $\approx 4\rho_0$. Decreasing the value of L has globally and systematically reduced the radius of the families of neutron stars. This is clear in figure 4.11, in that same figure we can see also that, for each family, the mass is also reduced by the decrease of L.

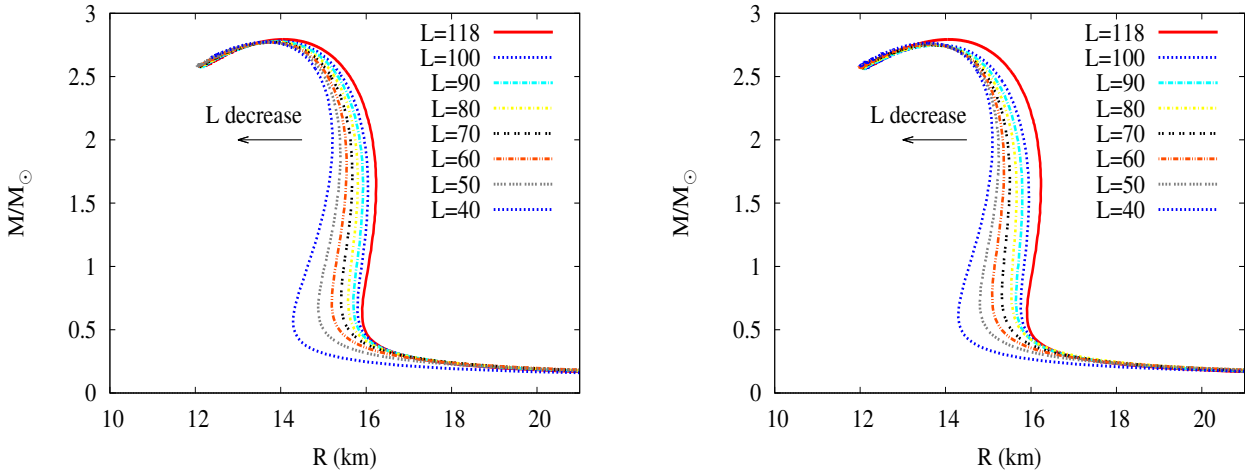

Figure 4.11: **Left**: $M/M_\odot$ dependence on the radius R in correspondence with the σ-ρ mixing term for different values of L. **Right**: $M/M_\odot$ dependence on the radius R in correspondence with ω-ρ mixing term for different values of L. Both mixings have a similar effect which is to generally reduce the radii of all calculated stars. The maximum mass is reduced also.

4.2.4 Possible neutron stars

The TOV equations predict families of stars, one for each EOS and, as we saw in subsection 4.2.3 the model predicts a very large array of possible stars but we will always have to compare them with observation. So here we have fixed the mass of observed stars, $1M_\odot$, $1.44M_\odot$ and $1.67M_\odot$ and then, varying the L parameter saw what happens to their radius. Figure 4.12 shows us that the influence of the nonlinear terms associated with Λ_ω and Λ_σ in the Lagrangian (4.1.1) force the radii of all the stars to decrease with increasing Λ_i. Also the the influence of the ω-ρ term is stronger in that effect, it hastens the decrease in the radius, more than the σ-ρ term. Stars with the same maximum radius have systematically more mass with the σ-ρ mixing than with the ω-ρ mixing. We now fix three masses for observed neutron stars, a $1\,M_\odot$, a pulsar of mass $1.44\,M_\odot$ [27] and the J903+0327 pulsar with $1.67\,M_\odot$ [28]. Using the masses as input from our solutions to the TOV equation we calculate how radii change with L. In figure 4.13 we plot the results. The radii decrease as L decreases. For masses larger than one solar mass the radius decreases linearly with the decrease of L. For a fixed mass, the effect of the σ-ρ produces a larger star radius than that with the ω-ρ mixing for the same L. We can see from figure 4.14 the neutron star with $1\,M_\odot$ will never reach the direct Urca process. Both the other two neutron stars will reach it for the range of L with corresponding Λ_i where $\rho_{\text{Urca}}/\rho_0$ is lower than ρ_c/ρ_0. The star with the largest mass also has the largest interval where $\rho_{\text{Urca}} < \rho_c$.

From the calculations that led to figure 4.14 we can build table 4.6 to be able to quantify the ranges in which the direct Urca process is allowed.

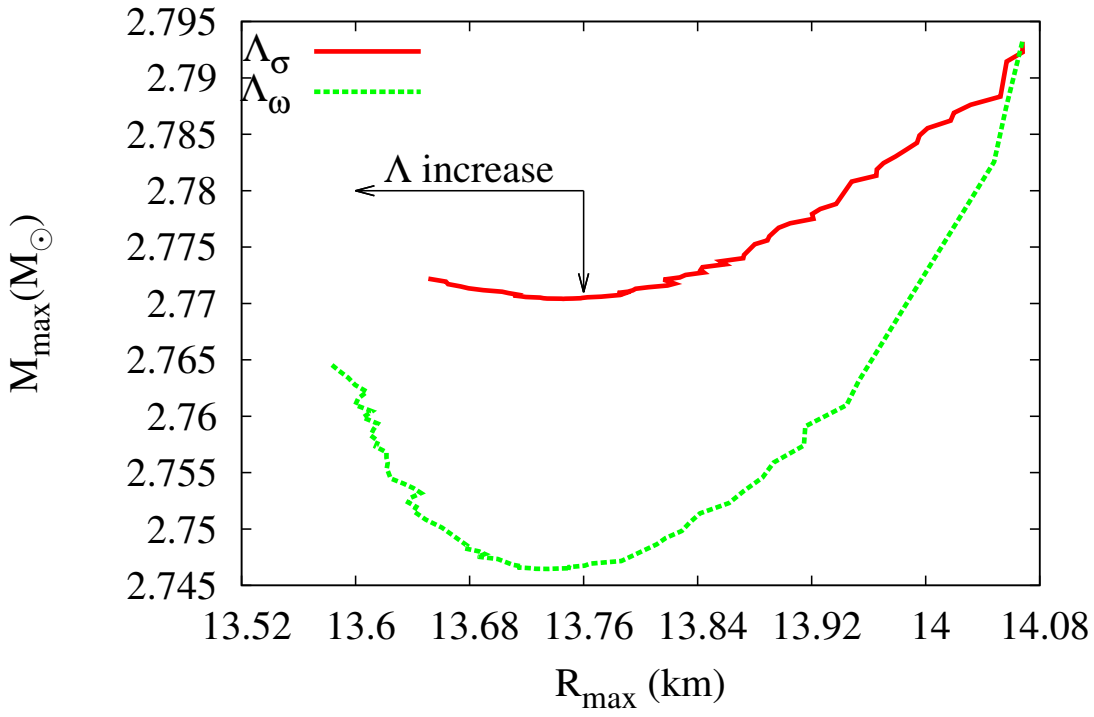

Figure 4.12: Maximum mass versus maximum radius. The Λ_σ (full line) and Λ_ω (dashed line) couplings grow from right to left and from top to bottom. L decreases in both these directions.

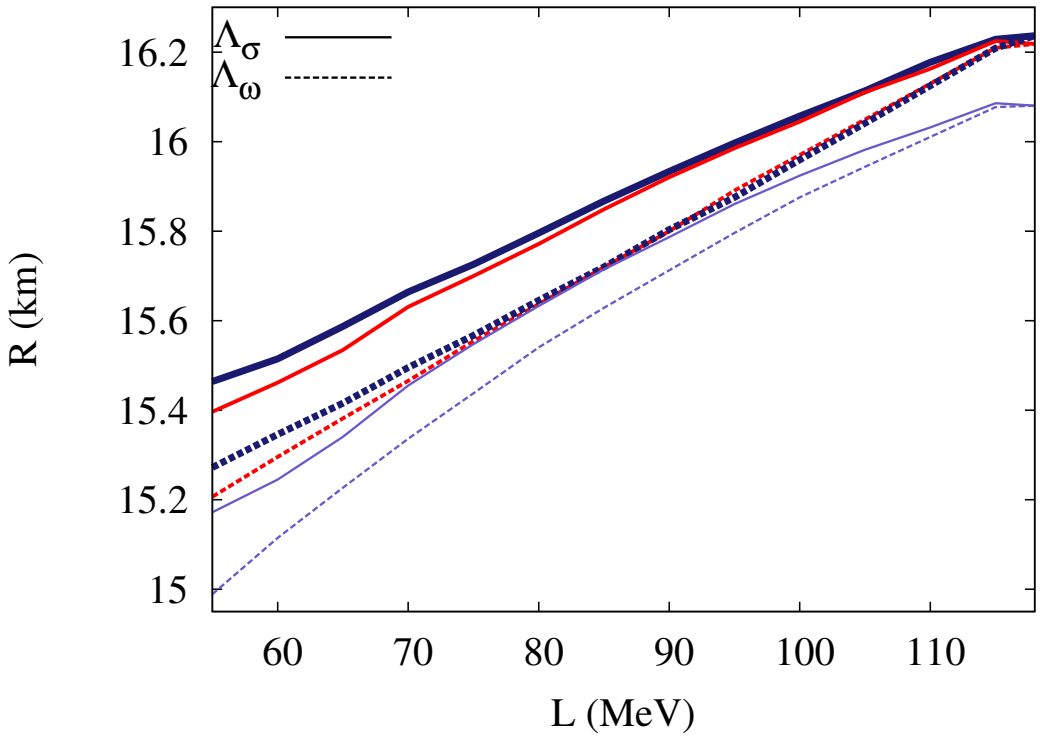

Figure 4.13: Radius versus L for three stars of masses $1\,M_\odot$, $1.44\,M_\odot$ and $1.67\,M_\odot$ with increasing line thickness as the mass grows. The σ-ρ mixing is a full line and the ω-ρ line is a dashed line.

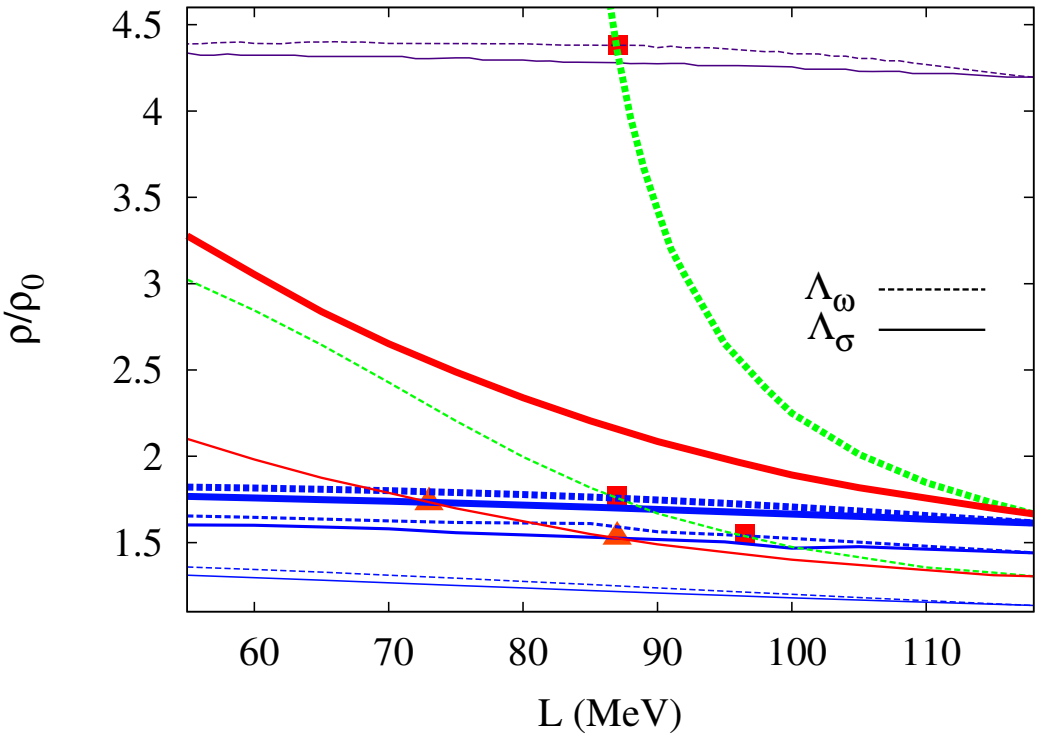

Figure 4.14: Neutron and proton matter in β equilibrium central density variation with L (in blue). This figure includes three stars of masses $1\,M_\odot$, $1.44\,M_\odot$ and $1.67\,M_\odot$ with increasing line thickness mass growth. Also plotted is the density of the onset of the direct Urca process for different L, in green is Λ_ω and in red is Λ_σ. Thin lines are $x_{\rm DU}$=1/9 and $x_{\rm DU}$ 0.148 are the thick lines. The central density for maximum mass stars is in purple. Triangles represent the intersection of σ-ρ mixing curves and squares the intersection of ω-ρ mixing curves.

x_{DU}	$1.44\,M_\odot$	$1.67\,M_\odot$	M_{max}
$1/9$,Λ_σ	$(73, 1.73)$	$(87, 1.53)$	-
$1/9$,Λ_ω	$(87.01, 1.77)$	$(96.5, 1.55)$	-
0.148,Λ_ω	-	-	$(87.1, 4.38)$

Table 4.6: Intersection points of the curves of $\rho_{\text{Urca}/\rho_0}$ and the central densities ρ_c/ρ_0 of the various masses of neutron stars and the two limits of the Urca process. Each point represents $(L, \rho/\rho_0)$ with L in MeV.

From figure 4.14 and table 4.6 we can see that the $1.44\,M_\odot$ neutron star has enough density to allow the direct Urca process within the range $L \in [73, 118]$ MeV for the σ-ρ mixing and in the range $L \in [87.01, 118]$ MeV for the ω-ρ mixing. The $1.67\,M_\odot$ neutron star has enough density to allow the direct Urca process within the range $L \in [87, 118]$ MeV for the σ-ρ mixing and in the range $L \in [96.5, 118]$ MeV for the ω-ρ mixing. Maximum mass stars allow the direct Urca process for all calculated L in any mixing. The $1\,M_\odot$ neutron star hasn't got enough central density to allow cooling with direct Urca process, but the Urca process is not the only way neutron stars cool down. The Urca process is not the only way through which neutron stars can cool down, they also cool down by losing energy in the form of radiation among other processes. If all neutron stars lose matter as they evolve then we could infer that the $1\,M_\odot$ neutron star is an older star than the pair of $1.44\,M_\odot$ and $1.67\,M_\odot$ neutron stars. If we knew how much matter they lose as a function of time then we could know how old they are just by knowing their mass.

4.2.5 Strange stars

The inclusion of hyperons in the calculations change the way everything works, from charge neutrality to mass-radius profiles. Figure 4.15 lets us see how charge neutrality works in this case (let us look at only the original NL3 set, the thick lines): at low densities the charged particles are only the protons and electrons in equal numbers and, from the moment these two densities start to differ muons appear to compensate for the imbalance. Then, at about $\rho \approx 1.8\rho_0$ the Σ^- baryon starts to appear to compensate for the great fall in electron and muon numbers. At approximately $\rho \approx 2\rho_0$ the total number of charged particles is too low and to compensate for this loss, the neutral baryon Λ^0 appears and rises fast until it stabilizes at $\rho \approx 4\rho_0$. At $\rho \approx 3\rho_0$ the number of Σ^- lowers enough for the baryon Ξ^- make its appearance. Proton populations are reduced by $\rho \approx 4\rho_0$ and the Σ^+ appears to keep charge neutrality. We can see in the same figure that the lowering of the slope of the symmetry will make all the hyperons onset happen at higher densities in this mixing except for the Σ^- which appears at a slightly lower density. Muon, proton and electron populations are lowered at most densities when $L = 55$ MeV in relation to $L = 118$ MeV. The same happens for all charged baryons except for Σ^- whose production is greater with $L = 55$ MeV than with $L = 118$ MeV. Neutron populations rise for $L = 55$ MeV at densities higher

than $\rho \approx \rho_0$ and all neutral baryons (except neutrons) appear at a higher density in comparison with the original $L = 118$ MeV. The Urca cooling process appears at a higher density for $L = 55$ MeV than for $L = 118$ MeV. Figure 4.15 is plotted for only one set of hyperon potentials. Were we to plot any other set the behaviour would change by having different charged hyperon onsets and, in some cases, some charged hyperons may not appear. The main particle fraction trend and charge neutrality is shown here.

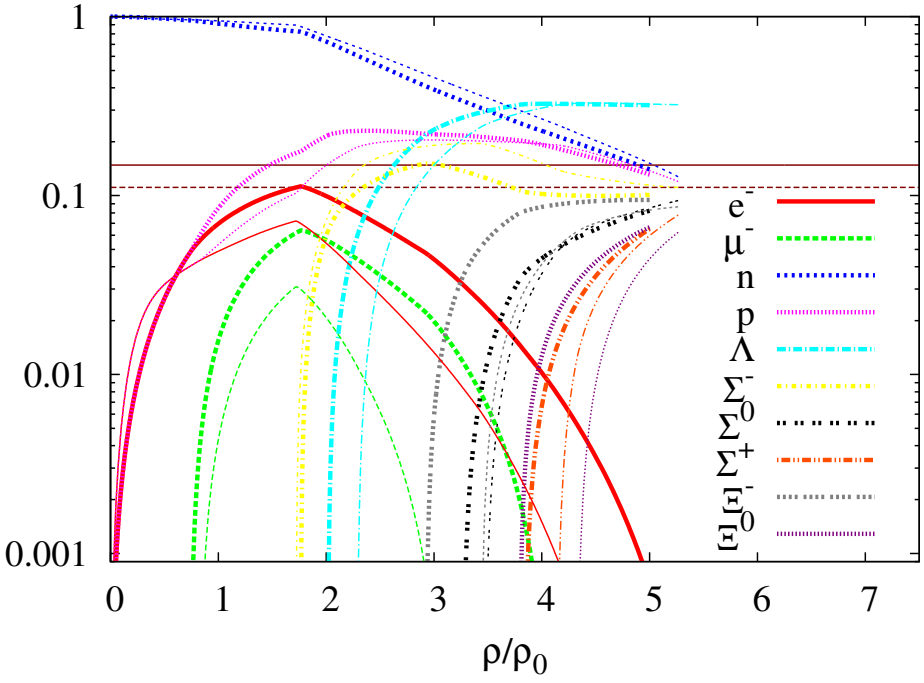

Figure 4.15: Particle fractions versus density when the model includes hyperons for the original NL3 parameter set ($L = 118$ MeV, thick lines) and for $L = 55$ MeV (thin lines). The horizontal lines mark the Urca process limits, a full line for the upper limit $U_{\text{sup}} = 0.148$ and a dashed line for the lower limit $U_{\text{sup}} = 1/9$. This is done only for one set of hyperon potentials.

In figure 4.16 we can see that having $L = 55$ MeV reduces the radii of neutron stars in comparison with $L = 118$ MeV for all calculated hyperon potentials. To distinguish the differences for both mixings at $L = 55$ MeV we have drawn figure 4.17. In this figure discern differences in the maximum mass for the two mixings, being highest (in any hyperon potential) for the ω-ρ mixing than for the σ-ρ mixing. The maximum radius is more reduced with the ω-ρ mixing than for the σ-ρ mixing and the difference is very tenuous.

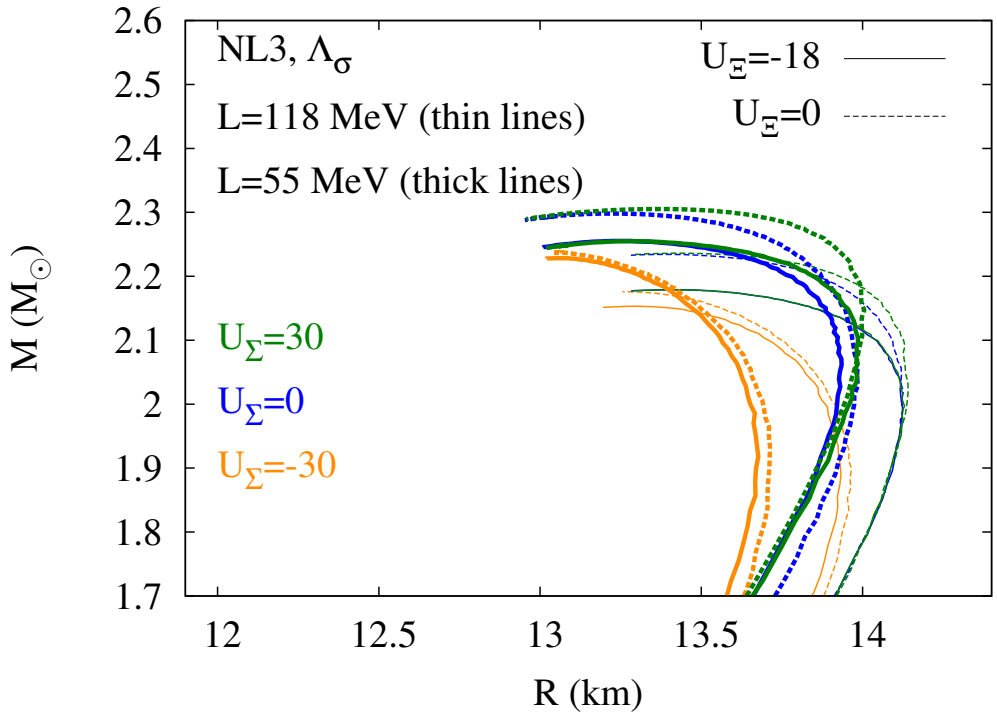

Figure 4.16: Neutron star mass versus radius different hyperon potentials. Both mixings reduce radii and increase mass with for any of the hyperon potentials. Here we show the σ-ρ mixing, approximately the same happens for the ω-ρ mixing.

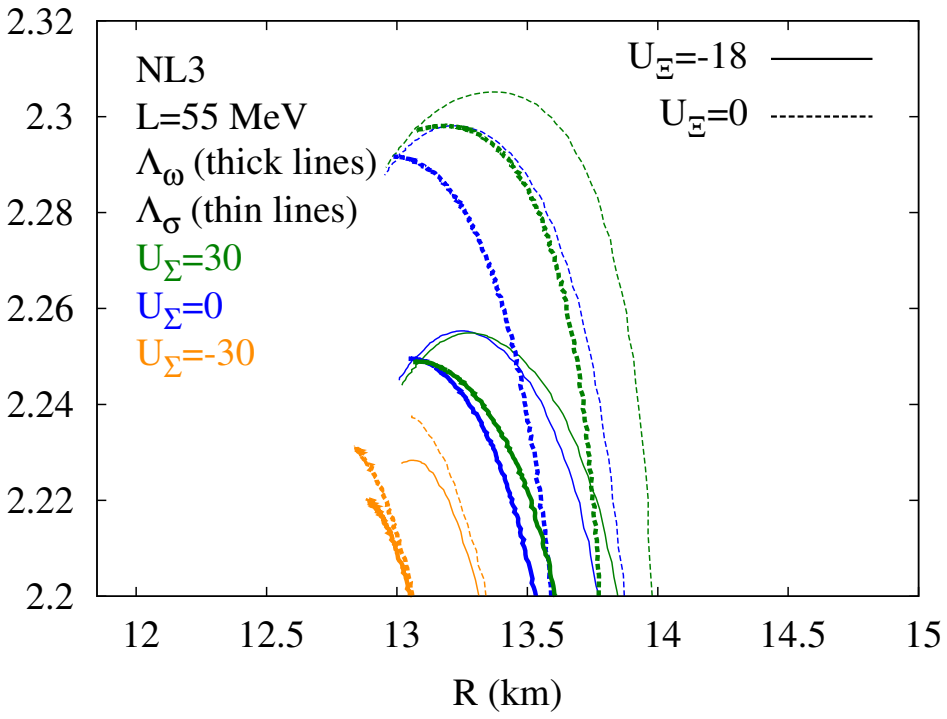

Figure 4.17: Neutron star mass versus radius for different hyperon potentials and meson mixings. The σ-ρ mixing are the thin lines and the ω-ρ are the thick lines.

Chapter 5

CONCLUSIONS

Neutron stars are objects of a very high density, to know their structure we must solve the TOV equations and for this we must have knowledge the high density nuclear EOS. In this work we use relativistic mean field theory to build an equation of state and calculate all the other variables such as saturation density, symmetry energy, slope of the symmetry energy, incompressibility, effective mass, etc. The main part of this work is the study of the effect of symmetry energy on the radius and mass of neutron stars and for that we change the NLWM+leptons+hyperons Lagrangian density by adding the term

$$g_\rho^2 \vec{\rho}_\mu \cdot \vec{\rho}^\mu \left[\Lambda_\sigma g_\sigma^2 \sigma^2 + \Lambda_\omega g_\omega^2 \omega_\mu \omega^\mu\right] \tag{5.0.1}$$

which changes the EOS and the density dependence of the symmetry energy. We have seen that the increase in each Λ_ω or Λ_σ decreases the symmetry energy slope L, at ρ_0. The EOS obtained from this theory is fitted to normal nuclear matter and the information conveyed by it is trustworthy in that range of densities. The fact that we can make it describe high density nuclear matter is mathematically sound but physically unknown and should be put to the test of observation. Our conclusions:

- Decreasing L means softening of the a_{sym} and that reduces both the maximum mass and the maximum radius of neutron stars made up of neutrons, protons electrons and muons in β equilibrium. This is accompanied by a reduction of the charged particle fractions at all densities.

- The calculated radii for the selected set of observed stars($1M_\odot$, $1.44M_\odot$ and $1.67M_\odot$) is in the range 14.8 to 16.2 km. This means that if observations are to disprove this theory, they should find neutron stars with radii in a different range than this. For masses larger than $1M_\odot$ the radius decreases linearly with L.

- The central densities of even the smallest neutron star admitted ($1M_\odot$) is in the range 1.14-1.38 ρ_0 and thereby allowing, according to theory, the existence of $p+n+e+\mu$ inside. So, all the stars considered in the present study are formed by n, p, e^- and μ^-.

- The onset of the URCA process is reached at higher densities with lower L.

- The μ^- onset density does not depend on L.
- Both the radius and the mass of neutron stars vary more with L if the ω-ρ term rather than the σ-ρ term is included.
- All maximum mass stars reach the direct Urca process in both mixings.
- The $1.44\,M_\odot$ neutron star has enough density to allow the direct Urca process within the range $L \in [73, 118]$ MeV for the σ-ρ mixing and in the range $L \in [87.01, 118]$ MeV for the ω-ρ mixing.
- The $1.67\,M_\odot$ neutron star has enough density to allow the direct Urca process within the range $L \in [87, 118]$ MeV for the σ-ρ mixing and in the range $L \in [96.5, 118]$ MeV for the ω-ρ mixing.
- The $1\,M_\odot$ neutron star has not enough density to allow for cooling by the Urca process.

For hyperons in any potential:

- both mixings reduce the radii of the families of stars
- the influence of the ω-ρ mixing is greater than for the σ-ρ mixing.

Also, in a certain hyperon potential combination we have:

- the onset of the Urca process takes place at a higher density for lower values of L in any of the mixings
- the fraction of charged particles is globally reduced for lower L except for Σ^- which is increased
- charged hyperon onset is at higher densities with lower L except for Σ^- which is at a lower density

In future work we will consider a full analysis of the symmetry energy dependence on the density and other properties:

- with other parameter sets
- the influence of hyperons in more detail and the effect of strange mesons
- influence of low temperatures on the transition to a cold neutron star
- the influence of rotation
- consider what is the role of quark deconfinement, if there is any

These and many other questions arise in theoretical study of neutron stars.

Appendix A

Units

Throughout this work we use natural units, i.e.

$$1 = \hbar = 6.5821 \times 10^{-16} \text{ eV s} \tag{A.0.1a}$$

$$1 = c = 2.9970 \times 10^{10} \text{ cm/s} \tag{A.0.1b}$$

$$1 = k_B = 1.3807 \times 10^{-16} \text{ erg/K} \tag{A.0.1c}$$

$$1 = G = 6.6720 \times 10^{-8} \text{ cm}^3\text{g}^{-1}\text{s}^{-2} \tag{A.0.1d}$$

The most used numerical result for conversions in this work is

$$\hbar c = 197.3 \text{ MeV fm} \tag{A.0.2}$$

Appendix B

Main theoretical procedures

B.1 Equations of motion

These are the equations of motion obtained from the main Lagrangian

$$\begin{cases} \left[\gamma_\mu \left(i\partial^\mu - g_\omega \omega^\mu - \frac{g_\rho}{2}\vec{\tau}\cdot\vec{\rho}^{\,\mu}\right) - (m_i - g_\sigma\sigma)\right]\psi_i = 0 \\ \partial_\alpha\partial^\alpha\sigma = -m_\sigma^2\sigma - \frac{\kappa}{2}\sigma^2 - \frac{\lambda}{6}\sigma^3 + 2\Lambda_\sigma g_\rho^2 \vec{\rho}_\mu\cdot\vec{\rho}^{\,\mu} g_\sigma^2\sigma + g_\sigma\sum_i \bar{\psi}_i\psi_i \\ \partial_\alpha\Omega^{\alpha\beta} = -g_\omega\sum_i\bar{\psi}_i\gamma^\beta\psi_i + m_\omega^2\omega^\beta + \frac{\xi}{6}g_\omega^4\omega_\mu\omega^\mu\omega^\beta + 2\Lambda_\omega g_\rho^2\vec{\rho}_\mu\cdot\vec{\rho}^{\,\mu}g_\omega^2\omega^\beta \\ \partial_\alpha\vec{R}^{\alpha\beta} = -\frac{g_\rho}{2}\sum_i\bar{\psi}_i\vec{\tau}\gamma^\beta\psi_i + m_\rho^2\vec{\rho}^{\,\beta} + 2g_\rho^2\vec{\rho}^{\,\beta}\left[\Lambda_\omega g_\omega^2\omega_\mu\omega^\mu + \Lambda_\sigma g_\sigma^2\sigma^2\right] \end{cases} \tag{B.1.1}$$

B.2 MFA equations of motion

We now make the mean-field approximation

$$\begin{cases} \sigma(x) \to \langle\sigma(x)\rangle = \sigma_0 = \sigma \\ \omega_\mu(x) \to \langle\omega_\mu(x)\rangle = \delta_{\mu0}\omega_0 = \omega \\ \vec{\rho}_\mu(x) \to \langle\vec{\rho}_\mu(x)\rangle = \delta_{\mu0}\delta^{i3}\rho_0^3 = \rho_{03} \end{cases} \tag{B.2.1}$$

Which in turn transform the equations of motion in

$$\begin{cases} g_\sigma\sum_i\langle\bar{\psi}_i\psi_i\rangle + 2\Lambda_\sigma g_\rho^2\rho_{03}^2 g_\sigma^2\sigma = m_\sigma^2\sigma + \frac{\kappa}{2}\sigma^2 + \frac{\lambda}{6}\sigma^3 \\ g_\omega\sum_i\langle\bar{\psi}_i\gamma^0\psi_i\rangle = m_\omega^2\omega + \frac{\xi}{6}g_\omega^4\omega^3 + 2\Lambda_\omega g_\rho^2\rho_{03}^2 g_\omega^2\omega \\ \frac{g_\rho}{2}\sum_i\langle\bar{\psi}_i\tau_i\gamma^0\psi_i\rangle = m_\rho^2\rho_{03} + 2g_\rho^2\rho_{03}\left[\Lambda_\omega g_\omega^2\omega^2 + \Lambda_\sigma g_\sigma^2\sigma^2\right] \end{cases} \tag{B.2.2}$$

For the Dirac equation we can now write, with the new definitions for the mesons

$$\left[\gamma_\mu\left(i\partial^\mu - g_\omega\omega^\mu - \frac{g_\rho}{2}\vec{\tau}\cdot\vec{\rho}^{\,\mu}\right) - (m_i - g_\sigma\sigma)\right]\psi_i(x) = 0 \tag{B.2.3}$$

B.3 Expectation values for operators in the ground state

In the MFA approach the nucleon fields satisfy an equation with no x-dependent terms allowing us to write

$$\psi_i(x) = \psi_i(k)e^{-ik\cdot x} \tag{B.3.1}$$

where

$$k\cdot x \equiv k_\mu x^\mu = k_0 t - \vec{k}\cdot\vec{r} \tag{B.3.2}$$

We then obtain

$$\left[\gamma_\mu\left(k^\mu - g_\omega\omega^\mu - \frac{g_\rho}{2}\tau_i\rho^{i\mu}\right) - (m_i - g_\sigma\sigma)\right]\psi_i(k) = 0 \tag{B.3.3}$$

Now we can make the definitions

$$\begin{aligned} K^\mu &= k^\mu - g_\omega\omega^\mu - \frac{g_\rho}{2}\tau_i\rho^{i\mu} \\ m_i^* &= m_i - g_\sigma\sigma \end{aligned} \tag{B.3.4}$$

transforming the Dirac equation (B.3.3) in

$$\left[\not{K} - m_i^*\right]\psi_i(k) = 0 \tag{B.3.5}$$

Using the properties of gamma matrices we can find

$$\left[K_\mu K^\mu - m_i^*\right]\psi_i(K) = 0 \tag{B.3.6}$$

Now we have a numerical equation, that is, the operator on the left has now become a number that multiplies another number $\psi_i(K)$ to give 0 and that means

$$K_0 = \sqrt{\vec{K}^{\,2} + m_i^{*2}} \tag{B.3.7}$$

Denoting the time component of the four vector $k \equiv (k^0, \vec{k})$ by

$$e(\vec{k}) \equiv k_0(\vec{k}) = K_0 + g_\omega\omega_0 + \frac{g_\rho}{2}\tau_i\rho^{i0} \tag{B.3.8}$$

the nucleon eigenvalues of 3-momentum $\vec{k}$ for particle and antiparticle are

$$e(\vec{k}) = E(\vec{k}) + g_\omega \omega_0 + \frac{g_\rho}{2}\tau_i \rho^{i0}$$
$$\bar{e}(\vec{k}) = E(\vec{k}) - g_\omega \omega_0 - \frac{g_\rho}{2}\tau_i \rho^{i0} \tag{B.3.9}$$

with $E(\vec{k}) \equiv K_0 = \sqrt{(\vec{k} - g_\omega \vec{\omega} - \sum_{j=1}^{3} \frac{g_\rho}{2}\tau_i \rho^{ij})^2 + m_i^{*2}}$.
We could now construct the ground-state expectation values of the nucleon currents by constructing the nucleon spinors first. This can be done because the Dirac equation has the same form as the free equation; only the four-momentum and mass are shifted by the mean meson field values. Then the currents could be constructed with the spinors by matrix multiplication and summation over occupied nucleon states. This is not necessary because there is a more economical way of evaluating the ground state expectation values that avoids the construction of the spinors. A single-nucleon state in this theory is characterized by the momentum $\vec{k}$ and the spin and isospin projection which we denote together by κ. Off course, each neutron and proton momentum state can have one of two spin projections $\pm 1/2$. Let us denote by a round bracket the expectation value of an operator in a single-particle state, $(\bar{\psi}_i \Gamma \psi_i)_{\vec{k}_\kappa}$. The expectation value of an operator in the ground state of the many-nucleon system is

$$\langle \bar{\psi}_i \Gamma \psi \rangle = \sum_\kappa \int \frac{d\vec{k}}{(2\pi)^3} (\bar{\psi}_i \Gamma \psi_i)_{\vec{k}_\kappa} \Theta \left[\mu - e(\vec{k})\right] \tag{B.3.10}$$

where the sum κ is understood to be over the spin-isospin states of the occupied momentum states and $\Theta(x)$ is the unity step function. μ is the Fermi energy, we can also call it chemical potential.

B.4 Single particle expectation values

The operator Γ appearing in the integral is generally to be found also in the Dirac Hamiltonian. Use the Dirac equation (B.3.3) and remember that $\gamma_\mu k^\mu = \gamma_0 k_0 - \vec{\gamma} \cdot \vec{k}$. Isolate k_0 and find the *Dirac Hamiltonian*

$$H_D = \gamma_0 \left[\vec{\gamma} \cdot \vec{k} + g_\omega \gamma_\mu \omega^\mu + \frac{g_\rho}{2} \vec{\tau} \cdot \gamma_\mu \vec{\rho}^{\,\mu} + m_i^*\right] \tag{B.4.1}$$

Now, take the expectation value in a single-nucleon momentum state as defined above

$$\left(\psi_i^\dagger H_D \psi_i\right)_{\vec{k}_\kappa} = K_0(\vec{k}) = E(\vec{k}) + g_\omega \omega_0 + \frac{g_\rho}{2}\tau_i \rho^{i0} \tag{B.4.2}$$

In this example the result is independent of spin and isospin projection or, in other words, the momentum eigenstates are degenerate with occupation number 4. In other cases we may have to take κ into account in other ways. We can obtain expectation values of other operators by taking the derivatives (with respect to a variable of interest) of (B.4.2).

B.5 Symmetry energy formulae

To calculate the symmetry energy we can suppose that the Fermi momenta for the nucleons are separate, let us see the terms in the energy density that can be turned into explicit functions of them

$$\frac{2}{\pi^2}\int_0^k k^2\sqrt{k^2+(m-g_\sigma\sigma)^2}\,dk = \frac{1}{\pi^2}\int_0^{k_n} k^2\sqrt{k^2+(m-g_\sigma\sigma)^2}\,dk + \\ +\frac{1}{\pi^2}\int_0^{k_p} k^2\sqrt{k^2+(m-g_\sigma\sigma)^2}\,dk \tag{B.5.1}$$

Let note that we can write $k_n = k_F\,(1+t)^{1/3}$ e $k_p = k_F\,(1-t)^{1/3}$, and then calculate

$$a_{sym} = \frac{1}{2}\left[\left(\frac{\partial^2\varepsilon/\rho}{\partial t^2}\right)\right]_{t=0} = \frac{1}{2\rho}\frac{2k_F^5}{9\sqrt{k_F^2+(m-g_\sigma\sigma)^2}} = \frac{k_F^2}{6\sqrt{k_F^2+(m-g_\sigma\sigma)^2}} \tag{B.5.2}$$

Q.E.D.

If we input the $\vec{\rho}_\mu$ field we must take into account

$$\frac{\partial^2}{\partial t^2}\left(\frac{1}{2\rho}m_\rho^2\rho_{03}^2\right) = \frac{\partial^2}{\partial t^2}\left(\frac{1}{2\rho}\left(\frac{m_\rho}{g_\rho}\right)^2\frac{1}{4}\left(\frac{g_\rho}{m_\rho}\right)^4(\rho_p-\rho_n)^2\right) = \\ = \frac{\partial^2}{\partial t^2}\left(-\frac{1}{8}\left(\frac{g_\rho}{m_\rho}\right)^2 t\,(\rho_n-\rho_p)\right) = \\ = \left(\frac{g_\rho}{m_\rho}\right)^2\frac{k_F^3}{12\pi^2} \tag{B.5.3}$$

After summing all, we get

$$a_{sym} = \left(\frac{g_\rho}{m_\rho}\right)^2\frac{k_F^3}{12\pi^2} + \frac{k_F^2}{6\sqrt{k_F^2+(m-g_\sigma\sigma)^2}} \tag{B.5.4}$$

When we mix $\vec{\rho}^{\,\mu}$ with ω^ν we get

$$a_{sym} = \frac{\rho_n+\rho_p}{\left(\frac{m_\rho}{g_\rho}\right)^2+2\Lambda\,(g_\omega\omega_0)^2} + \frac{k_F^2}{6\sqrt{k_F^2+(m-g_\sigma\sigma)^2}} \tag{B.5.5}$$

and almost the same thing happens when we mix $\vec{\rho}^{\,\mu}$ and σ.

Appendix C

Mathematical results

C.1 Integrals

$$\int_0^k \frac{mk^2}{\sqrt{k^2+m^2}}\,dk = \frac{1}{2}\left[mk\sqrt{k^2+m^2} - m^3\log\left(\frac{k+\sqrt{k^2+m^2}}{m}\right)\right] \tag{C.1.1}$$

$$\int_0^k \frac{m^2k^2}{(k^2+m^2)^{3/2}}\,dk = m^2\log\left(\frac{k+\sqrt{k^2+m^2}}{m}\right) - \frac{m^2k}{\sqrt{k^2+m^2}} \tag{C.1.2}$$

$$\int_0^k \frac{k^2}{\sqrt{k^2+m^2}}\,k^2dk = k^3\sqrt{k^2+m^2} + \frac{3}{8}\left[m^4\log\left\{\frac{k+\sqrt{k^2+m^2}}{m}\right\} - k\sqrt{k^2+m^2}(m^2+2k^2)\right] \tag{C.1.3}$$

$$\int_0^k k^2\sqrt{k^2+m^2}dk = \frac{1}{8}\left[k\sqrt{k^2+m^2}\left(m^2+2k^2\right) - m^4\log\left\{\frac{k+\sqrt{k^2+m^2}}{m}\right\}\right] \tag{C.1.4}$$

C.2 Differentiation

Let us denote

$$\vec{R}_{\mu\nu}\cdot\vec{R}^{\mu\nu} = R^i_{\mu\nu}R^{\mu\nu}_i \tag{C.2.1}$$

in which $\vec{R}_{\mu\nu} = \partial_\mu\vec{\rho}_\nu - \partial_\nu\vec{\rho}_\mu - g_\rho(\vec{\rho}_\mu\times\vec{\rho}_\nu)$ or

$$R^i_{\mu\nu} = \partial_\mu\rho^i_\nu - \partial_\nu\rho^i_\mu - g_\rho\varepsilon_{ijk}\rho^j_\mu\rho^k_\nu \tag{C.2.2}$$

Therefore, we can write

$$R^i_{\mu\nu}R^{\mu\nu}_i = \left(\partial_\mu\rho^i_\nu - \partial_\nu\rho^i_\mu - g_\rho\varepsilon_{ijk}\rho^j_\mu\rho^k_\nu\right)\left(\partial^\mu\rho^\nu_i - \partial^\nu\rho^\mu_i - g_\rho\varepsilon_{ijk}\rho^\mu_j\rho^\nu_k\right) \tag{C.2.3}$$

or still

$$\begin{aligned} R^i_{\mu\nu}R^{\mu\nu}_i = &\left(\partial_\mu\rho^i_\nu - \partial_\nu\rho^i_\mu\right)\left(\partial^\mu\rho^\nu_i - \partial^\nu\rho^\mu_i\right) + \\ &-g_\rho\varepsilon_{ijk}\rho^\mu_j\rho^\nu_k\left(\partial_\mu\rho^i_\nu - \partial_\nu\rho^i_\mu\right) \\ &-g_\rho\varepsilon_{ijk}\rho^j_\mu\rho^k_\nu\left(\partial^\mu\rho^\nu_i - \partial^\nu\rho^\mu_i\right) \\ &+g^2_\rho\varepsilon_{ijk}\varepsilon_{ilm}\rho^j_\mu\rho^k_\nu\rho^\mu_l\rho^\nu_m \end{aligned} \tag{C.2.4}$$

In our deductions above we must use the following derivatives

$$\frac{\partial\left(R^i_{\mu\nu}R^{\mu\nu}_i\right)}{\partial\left(\partial_\alpha\rho^a_\beta\right)} \tag{C.2.5a}$$

$$\frac{\partial\left(R^i_{\mu\nu}R^{\mu\nu}_i\right)}{\partial\rho^a_\beta} \tag{C.2.5b}$$

(C.2.5a) becomes

$$\begin{aligned} \frac{\partial\left(R^i_{\mu\nu}R^{\mu\nu}_i\right)}{\partial\left(\partial_\alpha\rho^a_\beta\right)} = &\,4\left(\partial^\alpha\rho^\beta_a - \partial^\beta\rho^\alpha_a\right) \\ &-g_\rho\varepsilon_{ajk}\left(\rho^\alpha_j\rho^\beta_k - \rho^\beta_j\rho^\alpha_k\right) \\ &-g_\rho\varepsilon_{alm}\left(\rho^l_\alpha\rho^m_\beta - \rho^l_\beta\rho^m_\alpha\right) \end{aligned} \tag{C.2.6}$$

(C.2.5b) becomes

$$\begin{aligned} \frac{\partial\left(R^i_{\mu\nu}R^{\mu\nu}_i\right)}{\partial\rho^a_\beta} = &-g_\rho\varepsilon_{iak}\rho^k_\nu\left(\partial^\beta\rho^\nu_i - \partial^\nu\rho^\beta_i\right) \\ &-g_\rho\varepsilon_{ija}\rho^j_\mu\left(\partial^\mu\rho^\beta_i - \partial^\beta\rho^\mu_i\right) \\ &-g_\rho\varepsilon_{iam}\rho^\nu_m\left(\partial_\beta\rho^i_\nu - \partial_\nu\rho^i_\beta\right) \\ &-g_\rho\varepsilon_{ila}\rho^\mu_l\left(\partial_\mu\rho^i_\beta - \partial_\beta\rho^i_\mu\right) \\ &+g^2_\rho\Big[\varepsilon_{iak}\varepsilon_{ilm}\rho^k_\nu\rho^\beta_l\rho^\nu_m \\ &+\varepsilon_{ija}\varepsilon_{ilm}\rho^j_\mu\rho^\mu_l\rho^\beta_m \\ &+\varepsilon_{ijk}\varepsilon_{iam}\rho^\beta_j\rho^k_\nu\rho^\nu_m \\ &+\varepsilon_{ijk}\varepsilon_{ila}\rho^j_\mu\rho^\beta_k\rho^\mu_l\Big] \end{aligned} \tag{C.2.7}$$

The Levi-Civita symbol obeys the following property

$$\varepsilon_{xyz}\varepsilon_{zwv} = \delta_{xw}\delta_{yv} - \delta_{xv}\delta_{yw} \tag{C.2.8}$$

using it, we get

$$\begin{aligned}\frac{\partial\left(R^i_{\mu\nu}R^{\mu\nu}_i\right)}{\partial\rho^a_\beta} = &-g_\rho\varepsilon_{iak}\rho^k_\nu\left(\partial^\beta\rho^\nu_i-\partial^\nu\rho^\beta_i\right)\\ &-g_\rho\varepsilon_{ija}\rho^j_\mu\left(\partial^\mu\rho^\beta_i-\partial^\beta\rho^\mu_i\right)\\ &-g_\rho\varepsilon_{iam}\rho^\nu_m\left(\partial_\beta\rho^i_\nu-\partial_\nu\rho^i_\beta\right)\\ &-g_\rho\varepsilon_{ila}\rho^\mu_l\left(\partial_\mu\rho^i_\beta-\partial_\beta\rho^i_\mu\right)\\ &+g^2_\rho\Big[\rho^m_\nu\rho^\beta_a\rho^\nu_m-\rho^l_\nu\rho^\beta_l\rho^\nu_a\\ &\rho^l_\mu\rho^\mu_l\rho^\beta_a-\rho^m_\mu\rho^\mu_a\rho^\beta_m\\ &\rho^\beta_a\rho^m_\nu\rho^\nu_m-\rho^\beta_m\rho^a_\nu\rho^\nu_m\\ &\rho^l_\mu\rho^\beta_a\rho^\mu_l-\rho^a_\mu\rho^\beta_l\rho^\mu_l\Big]\end{aligned} \tag{C.2.9}$$

One other important differentiation begins with the definitions

$$\Omega_{\mu\nu}=\partial_\mu\omega_\nu-\partial_\nu\omega_\mu,\ \Omega_{\mu\nu}\Omega^{\mu\nu} \tag{C.2.10}$$

and we must calculate

$$\frac{\partial}{\partial(\partial_\alpha\omega_\beta)}\Omega_{\mu\nu}\Omega^{\mu\nu}. \tag{C.2.11}$$

Before advancing we can note

$$\Omega_{\mu\nu}\Omega^{\mu\nu}=2\partial_\mu\omega_\nu\left(\partial^\mu\omega^\nu-\partial^\nu\omega^\mu\right) \tag{C.2.12}$$

and then

$$\begin{aligned}\frac{\partial}{\partial(\partial_\alpha\omega_\beta)}\Omega_{\mu\nu}\Omega^{\mu\nu} &= \\ =\frac{\partial}{\partial(\partial_\alpha\omega_\beta)}\left[2\partial_\mu\omega_\nu\left(\partial^\mu\omega^\nu-\partial^\nu\omega^\mu\right)\right] &= \\ =\left[2\delta_{\mu\alpha}\delta_{\nu\beta}\left(\partial^\mu\omega^\nu-\partial^\nu\omega^\mu\right)\right]+\left[2\partial_\mu\omega_\nu\left(g^{\mu\alpha}g^{\nu\beta}-g^{\mu\beta}g^{\nu\alpha}\right)\right] &= \\ =4\left(\partial^\alpha\omega^\beta-\partial^\beta\omega^\alpha\right)\end{aligned} \tag{C.2.13}$$

Bibliography

[1] James M. Lattimer and Madappa Prakash, Phys. Rep. **442**, 109 (2007)

[2] F. Özel, T. Güver, and D. Psaltis, ApJ **693**, 1775 (2009); F. Özel, G. Baym, and T. Guver, Phys. Rev. D **82**, 101301 (2010).

[3] A. W. Steiner, J. M. Lattimer, E. F. Brown, Astrophys. J. **722**, 33 (2010)

[4] K. Hebeler, J. M. Lattimer, C. J. Pethick, and A. Schwenk, Phys. Rev. Lett. **105**, 161102 (2010).

[5] N. K. Glendenning and S. A. Moszkowski, Phys. Rev. Lett. **67**, 2414 (1991)

[6] G. A. Lalazissis, J. König, *P. Ring, Phys. Rev. C* **55**, 540 (1997).

[7] König, J. and Ring, P., *Phys. Rev. Lett.* **71**, 3079–3082 (1993).

[8] Rafael Cavagnoli, Constança Providência, and Debora P. Menezes, Phys. Rev. C **83**, 045201 (2011).

[9] Camille Ducoin, Jérôme Margueron, Constança Providência, and Isaac Vidaña, *Phys. Rev. C* **83**, 045810 (2011)

[10] N. K. Glendenning, *Compact Stars*, Springer-Verlag, New-York, 2000.

[11] Fomin, N. et al, *Phys. Rev. Lett.* **108**, 092502 (2012)

[12] Johnson, M. H. and Teller, E., *Phys. Rev.* **98**, 783-787 (1955)

[13] Duerr, Hans-Peter, *Phys. Rev.* **103** 469-480 (1956)

[14] J. D. Walecka, *Ann. Phys.* **83** 491 (1974)

[15] B.D. Serot, J.D. Walecka, *Advances in Nuclear Physics* **16** (1986)

[16] B.D. Serot and J.D. Walecka, Adv. Nucl. Phys. **16** (1986) 1.; J. Boguta and A. R. Bodmer, Nucl. Phys. **A 292**, 413 (1977).

[17] Roca-Maza et al, *Phys. Rev. Lett.* **106** 252501 (2011)

[18] Warda, M. and Viñas, X. and Roca-Maza, X. and Centelles, M.,*Phys. Rev. C* **80**, 024316 (2009)

[19] K. Sumiyoshi, H. Kuwabara and H. Toki, Nuclear Physics **A581**, 725 (1995)

[20] P. Haensel et al, *Neutron Stars 1*, Springer-Verlag (2007)

[21] Yan, K.,*Progress in Geophysics* **21**, 38-47 (2006)

[22] Horowitz, C. J. and Piekarewicz, J., *Phys. Rev. Lett.* **86**, 5647–5650 (2001)

[23] G. Baym, C. Pethick, and P. Sutherland, *Astrophys. J.* **A175** 299 (1971)
P.J. Siemens, *Nucl. Phys.* **A141** 225 (1970)
G. Baym, H.A. Bethe and C.J. Pethick, *Nucl. Phys.* **A175** 225 (1971)

[24] Thorsson, V. and Prakash, M. and Tatsumi, T. and Pethick, C. J., *Phys. Rev. D* **52**, 3739–3741 (1995)

[25] J.M. Lattimer, C.J. Pethick, M. Prakash, P. Haensel *Phys. Rev. Lett.* **66** , 2701–2704 (1991)

[26] T. Klähn et al., *Phys. Rev. C* **74**, 035802 (2006)

[27] J.H. Taylor, J.M. Weisberg, *The Astrophysical Journal* **253** , 908-920 (1982)

[28] P. C. C. Freire, et al, *Monthly Notices of the Royal Astronomical Society* **412** 2763-2780 (2011)